Benemérita Universidad Autónoma de Puebla

Facultad de Ciencias Físico Matemáticas

A model of the radiation emitted by a source in the vicinity of a Kerr black hole

Tesis presentada al

Posgrado en Física Aplicada

como requisito parcial para la obtención del grado de

Doctor en Ciencias

por

M.C. Adriana González Juárez

Asesorada por

Dr. Gilberto Silva Ortigoza

Puebla Pue.
Junio de 2021

Benemérita Universidad Autónoma de Puebla

Facultad de Ciencias Físico Matemáticas

A model of the radiation emitted by a source in the vicinity of a Kerr black hole

Tesis presentada al

Posgrado en Física Aplicada

como requisito parcial para la obtención del grado de

Doctor en Ciencias

por

M.C. Adriana González Juárez

Asesorada por

Dr. Gilberto Silva Ortigoza

Puebla Pue.
Junio de 2021

Título: A model of the radiation emitted by a source in the vicinity of a Kerr black hole
Estudiante: M.C. Adriana González Juárez

COMITÉ

Dr. Gerardo Torres del Castillo
Presidente

Dr. Maximino Luis Arroyo Carrasco
Secretario

Dr. Carlos Ignacio Robledo Sánchez
Vocal

Dr. Miguel Chávez Dagostino
Jurado externo

Dr. Omar de Jesús Cabrera Rosas
Jurado externo

Dr. Enrique Pérez León
Suplente

Dr. Gilberto Silva Ortigoza
Asesor

Contents

Acknowledgments

I would like to express my deep gratitude to Dr. Gilberto Silva Ortigoza, my research supervisor, for approving the idea that gave rise to this thesis, for his patient guidance, enthusiastic encouragement, helpful corrections, for his invaluable humanity and friendship, and above all, for believing in me since before the beginning of the doctoral program.

I dedicate all the effort and results of this work to my blood and heart families, and to our loved ones who lost the battle against the pandemic. Without all your love, patience, support, example, advice and tireless desire to create happy moments, this would not have been possible. Thank you so much.

Abstract

The present thesis is the study of: the physics that characterizes the Bessel beams, the behavior of the reflected radiation by a parabolic mirror considering inclined incident light rays and Kirchhoff's diffraction theory applied to the phenomenon of reflection of light ray by a parabolic mirror, in particular that of the LMT/GTM antenna. It is shown that adiffractional beams which are invariant under translations along the axis of propagation, are characterized by a family of wavefronts and a caustic, and it is found that the caustic qualitatively coincides with the absolute maximum of the intensity pattern. Then, expressions for: the incident light rays and wavefronts, the reflected light rays, the reflected wavefronts, the caustic and the ronchigram have been obtained; those general results are applied to the parameters of the antenna of the LMT/GTM and it is shown that the caustic has a singularity of the hyperbolic umbilic type, which is locally stable under small perturbations of the optical system. The results presented could be associated to the radiation of a static source, in the geometrical optics limit. Finally, an expression for the intensity pattern associated with the reflection of a Bessel beam of order m by the LMT/GTM antenna has been determined; the preliminary results are presented.

Chapter 1

Introduction

The present thesis is a work that is developed within the area of the physics known as Geometrical Optics and Physical Optics, however, from the general objectives set out later and from the results that have been achieved so far, we observe that the next steps to solve the most general problem requires formal involvement with other areas of Physics such as, Optical Engineering, Observational Astrophysics and General Relativity, which means an enormous motivation for the continuity of the work and the initial stroke of the path by which the career of the presenting student, as a researcher, could develop.

In the framework of Physical Optics, an adiffractional beam is a solution to the wave equation in vacuum which has the property of self-reconstruction, that is, if the beam is blocked by a finite obstacle, after a certain distance from such an obstacle the beam reappears, and the property that it does not diffract as it propagates. Furthermore, using Kirchoff's diffraction theory, it has been numerically shown that it would be possible to generate the zero-order Bessel beam in the laboratory. Based on these results, this type of beam has been the subject of multiple investigations [1, 2, 3]. The more general objective that this research topic will look for to achieve in a near future, is to relate the types of beams described above to the radiation field emitted by a point source in the vicinity of the Schwarzschild and Kerr black holes. More specifically, we are interested in showing that, asymptotically, the beam associated with the cone of light at certain points in the Schwarzschild spacetime are of the zero-order Bessel type, whereas the beams corresponding to certain points of the Kerr spacetime are asymptotically of the Bessel type of order different from zero.

It is very important to remark that, the idea about that the reflection of a Bessel beam of order m corresponds, asymptotically, to the radiation emitted by a point-like source in the vicinity of a Kerr black hole, which obtains its angular momentum from the rotation of the black hole is a very strong **hypothesis**. The basis of this strong assumption is that modeling the radiation to be detected as a beam that has the property of vorticity is a good approach to start a study of this kind, and the simplest candidate is that of a Bessel beam.

Another hypothesis on that direcction is that the order of the beam would be associated with the specific angular momentum of the black hole. Although the rotation parameter is an arbitrary and continuous parameter, to take a case where it is determined by the order of the beam, that is, by a particular and discrete value, means that we are working, in first place, with a specific case where the black hole has a specific angular momentum. That problem will be formaly addressed in the near future. Thus, in chapter 2, we study the physics that characterizes the Bessel beams. Here we show that adiffractional beams are characterized by a family of wavefronts and a caustic or focus region which are invariant under translations along the axis of propagation.

It is important to note that the caustic qualitatively coincides with the absolute maximum of the intensity pattern. The work corresponding to this section of the thesis has been published in the refereed journal Physica Scripta [4].

Recently, a work was published in which the modification of the structure of the parabolic antenna of the Large Millimeter Telescope in Sierra Negra (LMT/GTM) was studied, to generate vortex beams and to use this configuration of the antenna to search for exoplanets [5]. In general, optical vortices have applications in various areas and size scales of knowledge as a study tool ranging from photons to astronomical scales [6]. In scalar theory, a vortex is a singularity of the wave characterized by having a singularity in phase and zero amplitude; furthermore, it has a rotating flow around this singularity. The work presented in chapter 3 corresponds to the study of the analogous problem to that of reflection of radiation by a vortex generator mirror, which is the behavior of the reflected radiation by a parabolic mirror considering inclined incident light rays. Here we have obtained expressions for: the incident light rays and wavefronts, the reflected light rays, the reflected wavefronts, the caustic and the ronchigram. Those general results are applied to the parameters of the antenna of the LMT/GTM and it is shown that the caustic has a singularity of the hyperbolic umbilic type, which is locally stable under small perturbations of the optical system. The results presented in this third chapter, could be associated to the radiation of a static source, in the geometrical optics limit, that is, from the information collected at the focal region, a ronchigram can be generated and to indicate whether the emitting source is static or not. The work developed in this section of the thesis has been published in the Journal of Optics Review [7].

The work that is presented in chapter 4 corresponds to the study of Kirchhoff's diffraction theory applied to the phenomenon of reflection of light ray by a parabolic mirror, in particular that of the LMT/GTM antenna, and to the determination of an expression for the intensity pattern associated with the reflection of a Bessel beam of order m by the LMT/GTM antenna. As a first step, the expression of light corresponding to a plane wave which incides on the antenna with certain inclination is computed. Then, it is assumed that the Bessel beam of order m is the superposition of many plane waves as many points are on a circle, and whose propagation vectors are on a cone. Because we are interested in the reflection of all the light rays of the resultant plane wave, we assume that the reference plane wavefront associated with this plane wave is given by the parameters of the antenna. Then, using this information, we obtain an integral expression for the scalar optical field associated with the reflection of a Bessel beam of order m by the LMT/GTM antenna, and finally, on certain appoximations we obtain an expression for the intensity pattern of that reflected radiation. Graphics corresponding to preliminary results on the behavior of the intensity pattern for the cases of zero order and $m = 5$ Bessel beams are presented. It is observed that, in general, the behavior of the intensity pattern is oscillatory and that the maximum intensity for the non-zero order of the Bessel beam is displaced, that is, it appears in larger values of τ. We are working on the construction of this work as an article that could be considered for publication.

Finally, in chapter 5 we present the discussion and conclusions about the current results, as well as the scope presented by this research for near future and future work.

Chapter 2

Ideal Bessel beams

In 1987 Durnin [8] introduced the concept of a *nondiffracting beam* as an exact nonsingular solution of the scalar wave equation in free space such that its intensity pattern is invariant under translations along the axis of propagation. He remarked that this type of beam may have an extremely narrow intensity profile with an effective width as small as several wavelengths and yet possess an infinite depth of field. Furthermore, by using numerical simulations based on scalar diffraction theory, he shown that physically realizable finite aperture approximations to the exact solution can also possess an extremely large depth of field. Then Durnin, Miceli and Eberly [9] reported the first experimental investigation on this type of beam. They used a circular slit and a lens separated by its focal distance to correct the diffracting wavefront transforming it into conical waves and hence producing a propagating invariant transverse Bessel intensity pattern described by the Bessel function of order zero. Since then, there has been considerable research on the subject, both theoretical and experimental ones [10, 11]. There is an infinite number of nondiffracting beams, the physical properties of each one are determined by an arbitrary complex function $A(\beta) = O(\beta)e^{ig(\beta)}$ defined on the momentum space. There are four subsets of this type of beams, where $A(\beta)$ is completely determined, they correspond to: plane waves, Bessel, Mathieu and parabolic beams [12, 13, 14, 15]. They are determined by the *separable solutions of the wave equation in free space* with a dependence of the form $e^{i(k_z z-\omega t)}$ [16].

On the other hand, because of practical applications, one of the main problems in geometrical optics is to compute the wavefronts and caustics associated with the refraction or reflection of plane and spherical waves. Therefore, a natural question is what are the wavefronts and caustics associated with a nondiffracting beam? Using the ideas from geometrical optics on the refraction of a plane wave by an interface, in a recent work [1], it was shown that a nondiffracting beam is characterized by a one-parameter family of wavefronts and a caustic, which are invariant under translations along the axis of evolution of the beam. These general results were applied to the Bessel, Parabolic and Mathieu beams [1, 2, 3] to obtain their geometrical characterization. For the Airy beams, which also are nondiffracting ones, see for example the references [17, 18].

It is important to remark that the caustic has only one branch and in the case of the Bessel beam of order zero it coincides with the maximum of the intensity pattern. Since the intensity pattern associated with a given scalar optical field has many maxima we raise another natural question: is it possible to define a family of caustics as the maxima of a given intensity pattern? We do not already have a complete answer to this question; however, the main purpose of the work in this chapter is to give a partial answer to this important issue. That is, we first show that the intensity pattern of a nondiffracting beam determines, in a natural manner, a complete integral of both the eikonal and Laplace equations on the plane. Then to the intensity pattern we associate a two-parameter, $(\mathcal{C}, \mathcal{L})$, family of curves and a one-parameter, $\mathcal{L}$, family of caustics defined on the

plane. When they are unfolded into the three space they are two-dimensional surfaces such that when $\mathcal{L} = 0$ they reduce to the geometrical wavefronts determined in our previous works [1, 2, 3]. That is, the novelty of the results presented in this chapter is to introduce a new degree of freedom given by the parameter $\mathcal{L}$, which in particular, gives a geometrical characterization of the maxima of the intensity pattern of a given nondiffracting beam. Before continuing, we remark why we are interested in defining the family of caustics to be determined by the maxima of the intensity pattern of a given scalar wave field.

One of the main topics in optical applications is to design and construct optical systems that produce an image of a given object as good as the original object. As far as we know the best theory to compute the image of a given object is the Maxwell theory of the electromagnetic field. If the polarization effects are no important, scalar theory is usually employed. Even more, if the problem under study is such that the wavelength is not important then one can use the geometrical optics approximation. In the geometrical optics approximation an optical field; that is, that given by the Maxwell theory and the scalar wave theory are characterized by a particular family of light rays or wavefronts and in general a caustic. In the geometrical optics approximation the caustic is defined by the envelope of the light rays, which coincides with the singularities and self intersections of the corresponding wavefronts. Equivalently, the caustic is also defined by all the points in the space where the geometrical intensity goes to infinity [19]. For this reason, it is common to associate the caustic region with the absolute maximum of the intensity computed from the optical field or from the scalar wave field. However, in general it is not so, actually, in the best case, the caustic provides a qualitative description of the absolute maximum of the corresponding intensity.

It is important to remark that in the geometrical optics limit the geometrical caustic plays a major role in computing the image of a given object produced by an optical system. That image is computed by using the family of light rays that determine the caustic. That is, with a given caustic we have a particular family of light rays and a particular image of a given real object. In exactly the same way as the caustic gives a qualitative description of the intensity pattern of a given optical or scalar wave field, the image computed by using the geometrical light rays will be a qualitative description of the image computed by using the Maxwell theory or the scalar wave theory. In other words, the image computed by using the geometrical optics approximation will be a cartoon of the image computed by using either the Maxwell or scalar wave theories. From these facts we believe that a natural generalization of the geometrical caustic is given by all the maxima of the intensity pattern of a scalar wave field and this is the main contribution of the work presented in this chapter. We do not know at this moment if it could be a good generalization of the geometrical caustic for a Maxwell field; however in the conclusions we return to this issue. Thus, we restrict our attention to the nondiffacting scalar wave fields. Therefore, with each value of the new parameter $\mathcal{L}$, introduced in this chapter, determined by each maxima of the intensity pattern of a nondiffacting scalar wave field we have a particular family of light rays or wavefronts that will allow to construct a better image than that computed by using only the light rays determined by the geometrical optics approximation. That is, the proposal introduced here represents a better approximation than the geometrical one. This is the main motivation to use those values for the new degree of freedom $\mathcal{L}$ determined by the maxima of the corresponding intensity pattern.

To clarify these results we present the Bessel beam of order m, we find that for $m \neq 0$ the curves are deformations of circles, which reduce to circles for $m = 0$ and the caustic family for each value of m is a family of circles characterized by the parameter $\mathcal{L}$ that can be chosen in such a way that the caustics coincide with the maxima of the intensity pattern; that is, with the maxima of the square of the Bessel function of order m. In the three dimensional space the wavefronts for $m = 0$ and $\mathcal{L} = 0$ are cones and the caustic is along the z axis, for $m = 0$ and $\mathcal{L} \neq 0$ the surfaces

are hyperboloids of one sheet and the caustics are cylinders, for $m \neq 0$ and $\mathcal{L} = 0$ the wavefronts are deformations of cones and the caustic is a cylinder; while for $m \neq 0$ and $\mathcal{L} \neq 0$ the surfaces are deformations of hyperboloids of one sheet and the caustics are cylinders too.

Along this chapter, and in order to introduce the main ideas of this work, in section 2.1 following the reference [20] we present as clear as possible the essential steps to characterize the *real Bessel beam of order zero*. Thus, in subsection 2.1.1 we study the geometrical description of the refraction phenomenon of a plane wave by an axicon lens when the wave vector of the plane wave is on the axis of symmetry of the lens. That is, an axicon lens is assumed to be located at free space with its axis of symmetry along the Z axis, it is illuminated by a plane wave evolving along the Z axis too and the resulting refracted light rays, wavefronts and their associated caustic are computed. Then, in subsection 2.1.2 we present an approximated integral expression for the scalar field associated with the refraction of the plane wave by the axicon lens, which is written in terms of a one-parameter family of solutions of both the eikonal and Laplace equations in free space, then the intensity pattern associated with that field is computed. In this section we remark that for a given value of the coordinate Z, the geometrical caustic coincides with the absolute maximum of the intensity pattern of the refracted scalar field. In section 2.2 we show that the intensity of a monochromatic nondiffracting beam, which is an observable, is determined by a positive real function and a complete integral, $W(X, Y, \beta)$, of both the eikonal and Laplace equations on the plane. Using this result in a natural manner we associate a one-parameter family of one-dimensional wavefronts and a caustic to the intensity of a nondiffracting beam. Here we remark that these geometric objects are the projections to the plane of the wavefronts and the caustic associated with the nondiffracting beam introduced by Durnin reported in [1]. Furthermore, using the fact that $W(X, Y, \beta)$ is the generating function of a canonical transformation we associate a two-parameter family of one-dimensional curves and one-parameter family of one-dimensional caustics to the intensity pattern of a nondiffracting beam. In section 2.3 we show that in the case of the Bessel beam of order m the one-parameter family of caustics can be chosen in such a way that they be determined by the maxima of the intensity pattern.

2.1 Refraction of a plane wave by an axicon lens

Following the reference [20], in the first part of this section we present a geometrical description of the refraction of a plane wave by an axicon lens and in the second one, we use the Fresnell-Kirchhoff difraction formula to obtain the scalar field associated with the refracted plane wave.

2.1.1 Geometrical description: refracted wavefronts and caustic

We assume that in the three dimensional free space we have an axicon lens, with constant refraction index n, such that its flat face is on the plane $Z = 0$. Therefore, using cyllindrical coordinates (ρ, θ, Z) its conical surface is described by

$$\mathbf{r}(\rho, \theta) = \rho\hat{\rho} + (a - \rho)\cot\alpha\hat{z}, \tag{2.1}$$

where a and α are the parameters characterizing the axicon lens, see Figure 2.1.

Now we have a plane wave evolving along the Z axis. If $\mathbf{r_0} = \rho\hat{\rho}$ denotes the intersection of an arbitrary incident light ray, associated with the incident plane wave, and $\mathbf{X}$ is the vector position of an arbitrary point on the corresponding refracted light ray, then the optical path lenght $\tilde{\Phi}$, from a point on the reference plane $\mathbf{r_0} = \rho\hat{\rho}$ to the point $\mathbf{X}$ is equal to

$$\tilde{\Phi}(\mathbf{X}, \rho, \theta) = n(a - \rho)\cot\alpha + |\mathbf{X} - \mathbf{r}(\rho, \theta)|\,. \tag{2.2}$$

A direct computation shows that for fixed values of ρ and θ, Eq. (2.2) is a solution of the eikonal

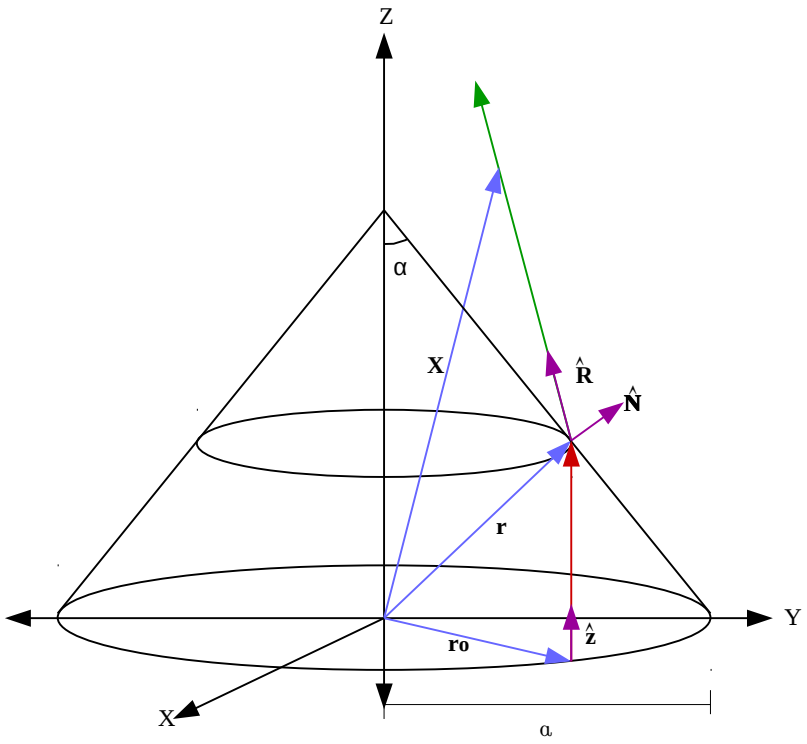

Figure 2.1: The axicon lens with parameters a and α. Furthermore, we show an incident light ray evolving in the direction $\hat{z}$, which intersects the reference plane $Z = 0$ at $\mathbf{r}_0$ and is refracted by the conical surface at the point $\mathbf{r}$. After the refraction the light ray evolves along $\hat{\mathbf{R}}$ direction; $\hat{\mathbf{N}}$ is the unit normal vector to the conical surface and $\mathbf{X}$ gives the position of a point on the refracted light ray.

equation in free space. That is,

$$\left(\frac{\partial\tilde{\Phi}}{\partial X}\right)^2+\left(\frac{\partial\tilde{\Phi}}{\partial Y}\right)^2+\left(\frac{\partial\tilde{\Phi}}{\partial Z}\right)^2=1. \tag{2.3}$$

This means that $\tilde{\Phi}$ is a complete integral of the eikonal equation. By definition, the wavefronts associated with this complete integral are given by all the points $\mathbf{X}$ such that

$$\tilde{\Phi}(\mathbf{X},\rho,\theta)=C, \tag{2.4}$$

where C is a real parameter. The refracted wavefronts are given by all the points, $\mathbf{X}$, in free space such that in addition to the condition (2.4), they also satisfy the following equations

$$\frac{\partial\tilde{\Phi}}{\partial\rho}=0, \qquad \frac{\partial\tilde{\Phi}}{\partial\theta}=0. \tag{2.5}$$

That is, the refracted wavefronts are given by the envelope of the wavefronts (2.4) determined by the complete integral (2.2). Therefore, using Eqs. (2.2), (2.4) and (2.5), a direct computation shows that the refracted wavefronts may be written in the following manner

$$\begin{aligned}\mathbf{X}(\rho,\theta,C) &= \{\rho+[C-n(a-\rho)\cot\alpha]\Omega\cos\alpha\}\hat{\rho}\\ &\quad+\{(a-\rho)\cot\alpha+[C-n(a-\rho)\cot\alpha](n+\Omega\sin\alpha)\}\hat{z},\end{aligned} \tag{2.6}$$

where

$$\Omega=-n\sin\alpha+\sqrt{1-n^2\cos^2\alpha}. \tag{2.7}$$

From Eq. (2.6) it is clear that the refracted wavefront train is locally described by a map between two subsets of $\mathcal{R}^3$ where (ρ, θ, C) are local coordinates labeling the points in the domain space and $\mathbf{X}=(X,\,Y,\,Z)$ are local coordinates labeling the points in the target space. The critical and caustic sets associated to this map will be computed using the following:

Definition: Let *h:* $\mathcal{M}\to\mathcal{N}$ be a differentiable map, with $\mathcal{M}$ and $\mathcal{N}$ differentiable manifolds. The set of points in $\mathcal{M}$ where h is not locally one-to-one is referred to as its critical set, and the image of the critical set is referred to as caustic set of h [22, 37].

Using Eq. (2.6), a direct computation shows that for this particular example, the critical set is given by

$$C = n(a-\rho)\cot\alpha-\frac{\rho\sec\alpha}{\Omega}, \tag{2.8}$$

and the caustic set, which is the image under the map (2.6) of the critical set is given by all the points (0, 0, Z_c) with

$$Z_c = \frac{2\csc(2\alpha)[a\Omega\cos^2\alpha-\rho(n\sin\alpha+\Omega)]}{\Omega}. \tag{2.9}$$

That is, the caustic is a segment of a line along the optical axis, in this case the Z axis. In Figure 2.2 we present the intersections with the plane $Y=0$ of: some incident light rays, the axicon lens, some refracted light rays, the caustic line and three refracted wavefronts.

2.1.2 The scalar field associated with the refracted plane wave

Now we assume that we have a plane wave evolving along the $\hat{z}$ direction inside the axicon lens given by

$$U(Z)=Ae^{ik_1Z}, \tag{2.10}$$

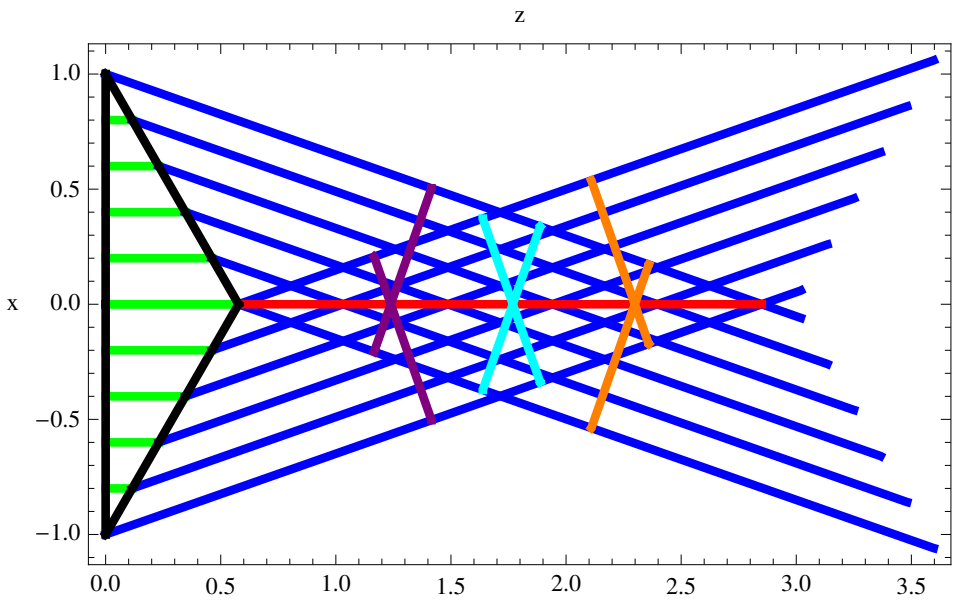

Figure 2.2: Here we present the intersections of some incident light rays (Green), the axicon lens (Black), some refracted light rays (Blue), the caustic line (Red) and three refracted wavefronts (Purple, Cyan, Orange) with the plane $Y = 0$. To obtain this plot we take $a = 1$, $n = 1.517$ and $\alpha = \pi/3$. The refracted wavefronts and refracted light rays are plotted using Eq. (2.6). The three wavefronts that we represent here correspond to $C = 1.5$ (Purple), $C = 2$ (Cyan) and $C = 2.5$ (Orange) and the caustic is plotted using Eq. (2.9).

with $k_1 = \omega/v_1$, v_1 is the speed of light inside the axicon lens, and A is a constant. Since $k_1 = (2\pi/\lambda_0)n = k_0 n$, then using the Fesnell-Kirchhoff formula, a direct computation shows that the refracted scalar optical field is given by

$$U(\mathbf{X}) = -\frac{iAk_0}{4\pi}\int_{-\pi}^{\pi}\int_0^a \frac{e^{ik_0\tilde{\Phi}}}{|\mathbf{X}-\mathbf{r}(\rho,\theta)|}[(n\hat{\mathbf{z}}+\hat{\mathbf{R}})\cdot\hat{\mathbf{N}}]\frac{\rho d\rho d\phi}{\sin\alpha}, \tag{2.11}$$

where $\hat{\mathbf{R}}$ gives the direction of the difracted-refracted ray,

$$\hat{\mathbf{N}} = \cos\alpha\,\hat{\rho} + \sin\alpha\,\hat{z}, \tag{2.12}$$

is the unit normal vector to the refracting conical surface and $\tilde{\Phi}$ is the optical path lenght given by Eq. (2.2). It is important to remark that the vector field $\hat{\mathbf{R}}$ is a function of the point $\mathbf{X}$, where the scalar optical field $U(\mathbf{X})$ is being evaluated and the points of the refracting cone; that is,

$$\hat{\mathbf{R}}(\mathbf{X},\rho,\theta) \equiv \frac{\mathbf{X}-\mathbf{r}(\rho,\theta)}{|\mathbf{X}-\mathbf{r}(\rho,\theta)|}. \tag{2.13}$$

Now observe that the optical path lenght (2.2) can be rewritten in the following manner

$$\tilde{\Phi}(\mathbf{X},\rho,\theta) = \mathbf{X}\cdot\hat{\mathbf{R}} - \mathbf{r}\cdot\hat{\mathbf{R}} + n(a-\rho)\cot\alpha. \tag{2.14}$$

In the above subsection, we have shown that the refracted wavefronts are determined by the envelope of the wavefronts associated with this optical path lenght. This is equivalent to replace the vector field $\hat{\mathbf{R}}(\mathbf{X},\rho,\theta)$ by $\hat{\mathbf{R}}_G$ given by the refraction law. A direct computation shows that for the axicon lens

$$\hat{\mathbf{R}}_G(\phi) = \Omega\cos\alpha\,\hat{\rho} + (n+\Omega\sin\alpha)\hat{z}. \tag{2.15}$$

Therefore, using Eqs. (2.11), (2.12) and (2.15) a direct computation shows that when $|\mathbf{X}-\mathbf{r}(\rho,\theta)| \to Z/[n+\Omega(\hat{z}\cdot\hat{\mathbf{N}})]$, the scalar field associated with the refracted plane wave can be written in the following manner

$$U(\mathbf{X}) = \frac{Ak_0a^2(\sin\alpha + n\sqrt{1-n^2\cos^2\alpha})}{8\pi Z\sin\alpha}\int_{-\pi}^{\pi} e^{ik_0\Phi_G}d\phi, \tag{2.16}$$

where Φ_G is obtained from Eq. (2.14) by replacing $\hat{\mathbf{R}}$ by $\hat{\mathbf{R}}_G$. That is,

$$\Phi_G = \mathbf{X}\cdot\hat{\mathbf{R}}_G(\phi) - a\Omega\cos\alpha - \frac{\pi}{2k_0}. \tag{2.17}$$

This means that the scalar field (2.16) is determined by a one-parameter family of solutions of both the eikonal and Laplace equations in free space given by Eq. (2.17). This fact was used in [1] to associate to a nondiffracting beam a one-parameter family of wavefronts and a caustic. Finally, we find that the intensity for the refracted scalar field is given by

$$I = \left[\frac{Aa^2k_0(\sin\alpha + n\sqrt{1-n^2\cos^2\alpha})}{4Z\sin\alpha}J_0(k_0\Omega\cos\alpha\sqrt{X^2+Y^2})\right]^2, \tag{2.18}$$

where J_0 is the Bessel function of order zero. We finish this section by remarking two facts. First, the refracted scalar field associated with the refraction of a plane wave by an axicon lens given by (2.16) is the superposition of many monochromatic plane waves, as many values the coordinate ϕ takes, with amplitude $[Ak_0a^2(\sin\alpha + n\sqrt{1-n^2\cos^2\alpha})]/(8\pi Z\sin\alpha)$ and spatial phase given by $k_0\Phi_G$. Second, for a given value of Z the *absolute maximum* of the intensity (2.18) is given by $X = 0$ and $Y = 0$, which coincides with the geometrical caustic. In figure 2.3 we show the intensity pattern given by Eq. (2.18) for $Ak_0^2 = 1$, $a = 1$, $n = 1.517$, $\alpha = \pi/3$ and $k_0Z = 1.5$ and the corresponding caustic (0, 0, 1.5), which is a single point.

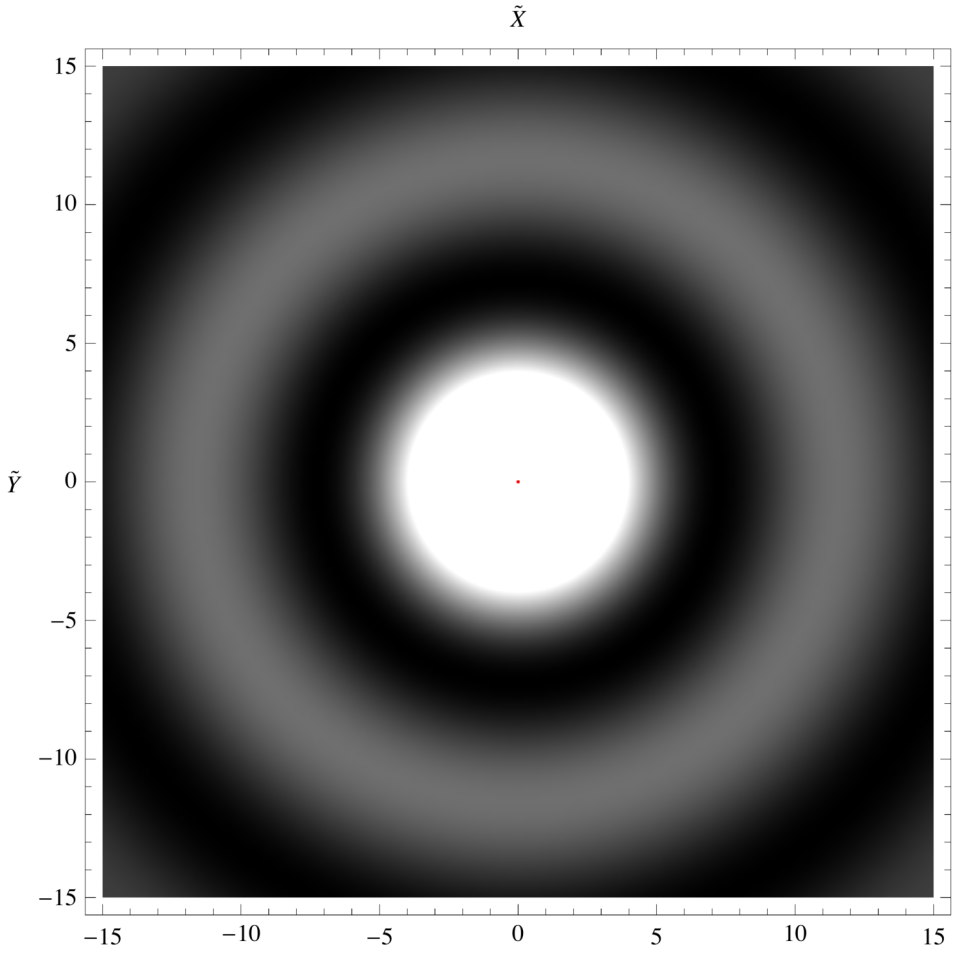

Figure 2.3: Here we present the intensity pattern given by Eq. (2.18) (GrayLevel) and the geometrical caustic (0, 0, 1.5), which is a single point (Red). To obtain this plot we take $Ak_0^2 = 1$, $a = 1$, $n = 1.517$, $\alpha = \pi/3$ and $k_0 Z = 1.5$. Furthermore, $\tilde{X} = k_0 X$ and $\tilde{Y} = k_0 Y$. Observe that the geometrical caustic coincides with the absolute maximum of the intensity pattern.

2.2 Curves, wavefronts and caustics determined by the intensity of an adiffractional beam

The solution of the wave equation in free space introduced by Durnin can be written in the following way [23]

$$\psi(\mathbf{X},t) \quad = \quad \int_{-\pi}^{\pi} O(\beta) e^{i[k_t(X cos\beta + Y \sin\beta) + k_z Z + g(\beta) - \omega t]} d\beta, \tag{2.19}$$

where $O(\beta)$ and $g(\beta)$ are arbitrary real functions of β, k_t and k_z are the transverse and longitudinal components of the wave vector $\mathbf{k}$ respectively (see Figure 2.4). From this expression it is clear that

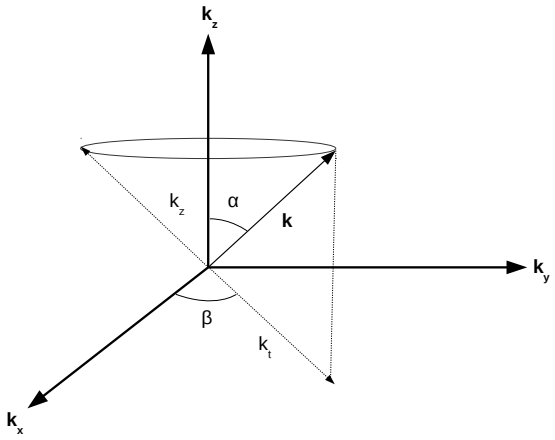

Figure 2.4: We show the wave vector $\mathbf{k} = k_0(\cos\beta \sin\alpha\, \hat{x} + \sin\beta \sin\alpha\, \hat{y} + \cos\alpha\, \hat{z}) = k_t(\cos\beta\, \hat{x} + \sin\beta\, \hat{y}) + k_z\, \hat{z}$, $k_t^2 + k_z^2 = \omega^2/c^2 = k_0^2$ and $-\pi \leq \beta \leq \pi$. Since k_t and k_z are given, then $\alpha = \arctan(k_t/k_z)$.

this solution is the superposition of many monochromatic plane waves with amplitude $O(\beta)$ and phase

$$\Phi(\mathbf{X},t,\beta) \quad \equiv \quad k_t(X cos\beta + Y \sin\beta) + k_z Z + g(\beta) - \omega t, \tag{2.20}$$

as many different values the coordinate β takes. For $k_t = 0$, Eq. (2.19) is a plane wave evolving along the Z axis; while for $0 < k_t < k_0$ the solution is a nondiffracting beam because, $\psi(\mathbf{X},t) = A(X,Y)e^{i(k_z Z - \omega t)}$, and thus its intensity profile

$$I(X,Y,Z) \quad = \quad |A(X,Y)|^2 = \left| \int_{-\pi}^{\pi} O(\beta) e^{ik_t W(X,Y,\beta)} d\beta \right|^2, \tag{2.21}$$

$$W(X,Y,\beta) \quad \equiv \quad X cos\beta + Y \sin\beta + \frac{g(\beta)}{k_t}, \tag{2.22}$$

does not depend on the Z coordinate; that is, it is invariant under translations along the $\hat{z}$ direction. Therefore, the intensity of a monochromatic nondiffracting beam, which is an observable, is determined by the positive real function $O(\beta)$ and a complete integral, $W(X,Y,\beta)$, of both the eikonal and Laplace equations on the plane. That is, from Eq. (2.22) a direct computation shows that

$$(\nabla W)^2 \quad = \quad 1, \tag{2.23}$$

$$\nabla^2 W \quad = \quad 0, \tag{2.24}$$

for each value of β (see also Reference [24]).

Since the Bessel beam of order zero is given by Eq. (2.19) with $O(\beta) = 1/2\pi$ and $g(\beta) = 0$, then

$$\psi(\mathbf{X}, 0) = \frac{1}{2\pi}\int_{-\pi}^{\pi} e^{i\mathbf{X}\cdot\mathbf{k}} d\beta. \tag{2.25}$$

Observe that this expression has the form of the field associated with the refraction of a plane wave for an axicon lens given by Eq. (2.16). That is, the scalar field (2.16) is the theoretical description of a real Bessel beam of order zero while that given by (2.25) is the ideal Bessel beam. Using this similarity in a recent work [1] we associated to the nondiffracting beam (2.19) a one-parameter family of wavefronts and a caustic, such beams are invariant under translations along the propagation axis. In the case of the Bessel beam of order zero the wavefronts are cones and their apexes determine the caustic line, which coincides with the Z axis; while the wavefronts of the theoretical description of the real Bessel beam of order zero given by Eq. (2.16) are finite cones and the caustic is a segment of a line on the Z axis too, see Figure 2.2. It is important to remark that the wavefronts and caustics determined by the real nondiffracting beams are finite surfaces with the same type of singularities as those determined by the ideal nondiffracting beams.

In the present chapter we give a generalization of the results presented in [1]. To this end, we focus our attention on the intensity of the nondiffracting beam given by Eq. (2.21). Since W given by Eq. (2.22) is a complete integral of the eikonal equation in free space, then in accordance with the procedure presented in the subsection 2.1 above, and that used in references [1, 25, 26] in a natural manner we associate a one-parameter family of wavefronts to the intensity pattern of the nondiffracting beam (2.21), given by all the points on the plane such that

$$W = Xcos\beta + Y\sin\beta + \frac{g}{k_t} = \frac{\mathcal{C}}{k_t}, \tag{2.26}$$

$$\frac{\partial W}{\partial \beta} = -Xsin\beta + Y\cos\beta + \frac{dg}{k_t d\beta} = 0, \tag{2.27}$$

where $\mathcal{C}$, is a real parameter. That is,

$$\begin{aligned} \tilde{x} &= (\mathcal{C} - g)\cos\beta + \left(\frac{dg}{d\beta}\right)\sin\beta, \\ \tilde{y} &= (\mathcal{C} - g)\sin\beta - \left(\frac{dg}{d\beta}\right)\cos\beta, \end{aligned} \tag{2.28}$$

where $\tilde{x} = k_t X$ and $\tilde{y} = k_t Y$. It is important to remark that Eqs. (2.28) describe *geometrical wavefronts*; that is, they are level curves of a new solution of the eikonal equation (2.23). Since Eqs. (2.28) describe a map between two subsets of $\mathcal{R}^2$ where ($\mathcal{C}$, β) are local coordinates in the domain space and ($\tilde{x}$, $\tilde{y}$) are local coordinates in the target space, then in accordance with the definition of critical and caustic sets of a differentiable map given above, a direct computation shows that the critical set of the map given by Eqs. (2.28); that is, the set of points in the domain space with coordinates ($\mathcal{C}$, β) such that the map is not locally one-to-one is given by

$$\mathcal{C} = g + \frac{d^2 g}{d\beta^2}. \tag{2.29}$$

Thus the caustic set, which is the image of the critical set under the map (2.28) is given by

$$\begin{aligned} \tilde{x}_c &= \left(\frac{d^2 g}{d\beta^2}\right)\cos\beta + \left(\frac{dg}{d\beta}\right)\sin\beta, \\ \tilde{y}_c &= \left(\frac{d^2 g}{d\beta^2}\right)\sin\beta - \left(\frac{dg}{d\beta}\right)\cos\beta. \end{aligned} \tag{2.30}$$

From Eq. (2.29) we have that if g determines a given critical set then $\tilde{g} = g + g_0$ also determines the same critical set, if and only if,

$$\frac{d^2 g_0}{d\beta^2} + g_0 = 0. \tag{2.31}$$

Therefore, we conclude that there is a family of complete integrals of both the eikonal and Laplace equations determined by $\tilde{g} = g + x_0 \cos\beta + y_0 \sin\beta$, with x_0 and y_0 constants, that has associated the same critical and caustic sets.

It is important to remark that the wavefronts (2.28) and the caustic (2.30) associated with the intensity of a nondiffracting beam (2.21) are the projections to the plane of those determined by the nondiffacting beam (2.19) reported in [1]. The generalization of those results follows from the following observation. The function W given by Eq. (2.22) is a complete integral of the eikonal equation in the plane. That is, it is a complete integral of the time-independent Hamilton-Jacobi equation for a free particle on the plane of unit mass and energy $E = 1/2$. Therefore, in accordance with the Hamilton-Jacobi theory it is the generating function of a canonical transformation such that

$$p_X = \frac{\partial W}{\partial X} = \cos\beta, \qquad p_Y = \frac{\partial W}{\partial Y} = \sin\beta, \tag{2.32}$$

$$Q_1 = \frac{\partial W}{\partial \beta} = -X \sin\beta + Y \cos\beta + \frac{dg}{k_t d\beta}, \tag{2.33}$$

where Q_1 is a new coordinate of the phase space. From Eqs. (2.27) and (2.33) we see that the Hamilton-Jacobi theory allows to give a generalization of the envelope definition. That is, instead of associating the one-parameter family of wavefronts (2.28) to the intensity pattern (2.21) of a nondiffracting beam, now we associate to it a two-parameter family of curves given by all the points (X, Y) on the plane such that

$$W = X \cos\beta + Y \sin\beta + \frac{g}{k_t} = \frac{\mathcal{C}}{k_t}, \tag{2.34}$$

$$\frac{\partial W}{\partial \beta} = -X \sin\beta + Y \cos\beta + \frac{dg}{k_t d\beta} = -\frac{\mathcal{L}}{k_t}, \tag{2.35}$$

where $\mathcal{C}$ and $\mathcal{L}$ are arbitrary real parameters. Or explicitly given by

$$\begin{aligned} \tilde{x} &= (\mathcal{C} - g)\cos\beta + \left(\frac{dg}{d\beta} + \mathcal{L}\right)\sin\beta, \\ \tilde{y} &= (\mathcal{C} - g)\sin\beta - \left(\frac{dg}{d\beta} + \mathcal{L}\right)\cos\beta. \end{aligned} \tag{2.36}$$

It is important to remark that the *geometrical wavefronts* are given by the particular value $\mathcal{L} = 0$. That is, they are level curves of a new solution of the eikonal equation (2.23). However, for $\mathcal{L} \neq 0$, they are not wavefronts because they do not correspond to the level curves of any solution to the eikonal equation. Observe that for a given value of $\mathcal{L}$ Eqs. (2.36) describe a map between two subsets of $\mathcal{R}^2$ where $(\mathcal{C}, \beta)$ are local coordinates in the domain space and $(\tilde{x}, \tilde{y})$ are local coordinates in the target space. The critical set of the map given by Eqs. (2.36); that is, the set of points in the domain space with coordinates $(\mathcal{C}, \beta)$ such that the map is not locally one-to-one is given by Eq. (2.29) too; that is, it is independent of the parameter $\mathcal{L}$. Thus the caustic set, which is the image of the critical set under the map (2.36) is given by

$$\begin{aligned} \tilde{x}_c &= \left(\frac{d^2 g}{d\beta^2}\right)\cos\beta + \left(\frac{dg}{d\beta} + \mathcal{L}\right)\sin\beta, \\ \tilde{y}_c &= \left(\frac{d^2 g}{d\beta^2}\right)\sin\beta - \left(\frac{dg}{d\beta} + \mathcal{L}\right)\cos\beta. \end{aligned} \tag{2.37}$$

In the same way a direct computation shows that the surfaces and caustics associated with the beam (2.19) in the three space, are given by

$$\begin{aligned}\tilde{x} &= (\mathcal{C}-g-\tilde{z})\cos\beta+\left(\frac{dg}{d\beta}+\mathcal{L}\right)\sin\beta,\\ \tilde{y} &= (\mathcal{C}-g-\tilde{z})\sin\beta-\left(\frac{dg}{d\beta}+\mathcal{L}\right)\cos\beta,\\ \tilde{z} &= \tilde{z},\end{aligned} \tag{2.38}$$

where $\tilde{z}=k_zZ$ and the caustics are given by

$$\begin{aligned}\tilde{x}_c &= \left(\frac{d^2g}{d\beta^2}\right)\cos\beta+\left(\frac{dg}{d\beta}+\mathcal{L}\right)\sin\beta,\\ \tilde{y}_c &= \left(\frac{d^2g}{d\beta^2}\right)\sin\beta-\left(\frac{dg}{d\beta}+\mathcal{L}\right)\cos\beta,\\ \tilde{z}_c &= \tilde{z}.\end{aligned} \tag{2.39}$$

From Eqs. (2.38) the surfaces can be written in the following manner: $\tilde{x}^2+\tilde{y}^2=(\mathcal{C}-g-\tilde{z})^2+(dg/d\beta+\mathcal{L})^2$. Thus, making $g=0$ and $\mathcal{L}=0$ for each value of $\mathcal{C}$ we have a cone with apex at $\tilde{z}=\mathcal{C}$ and for $g=0$ and $\mathcal{L}\neq 0$, for each value of $\mathcal{C}$, we have an hyperboloid of one sheet. Therefore, the geometrical meaning of the function $g(\beta)$ is to induce a deformation on those surfaces.

The main contribution in this chapter is to associate to the *intensity pattern of the nondiffracting beam* (2.21), a two-parameter family of one-dimensional curves characterized by the parameters $\mathcal{C}$ and $\mathcal{L}$ and a one-parameter family of caustics characterized by the parameter $\mathcal{L}$ given by Eqs. (2.36) and (2.37) respectively. Furthermore, we associate to the nondiffracting beam (2.19) a two-parameter family of surfaces and a one-parameter family of caustics given by Eqs.(2.38) and (2.39) respectively. It is important to remark that the parameter $\mathcal{L}$ appearing in the surfaces and caustics in principle can take any real value. As we see below in the case of a Bessel beam of order m, this parameter is chosen as the maxima of the square of the Bessel function of order m. In this way the intensity pattern of a Bessel beam of order m determines in a natural way a particular family of curves and caustics.

2.3 The Bessel beam of order m

The Bessel beam of order m is given by

$$\psi(\tilde{\rho},\tilde{\theta},\tilde{z},t) = e^{i(\tilde{z}+m\tilde{\theta}-\omega t)}J_m(\tilde{\rho}), \tag{2.40}$$

where m is an integer, $\tilde{\rho}=\sqrt{\tilde{x}^2+\tilde{y}^2}=k_t\sqrt{X^2+Y^2}$, $\tilde{\theta}=\arctan(\tilde{y}/\tilde{x})=\arctan(Y/X)$ and J_m is the Bessel function of order m. This beam is obtained from Eq. (2.19) with

$$\begin{aligned}O(\beta) &= \frac{1}{2\pi},\\ g(\beta) &= m\beta+\frac{3m\pi}{2}.\end{aligned} \tag{2.41}$$

Therefore, using Eqs. (2.21) and (2.41) a direct computation shows that the intensity profile for the Bessel beam of order m is given by

$$I(\tilde{x},\tilde{y},\tilde{z}) = J_m^2(\tilde{\rho}), \tag{2.42}$$

This means that the maxima of the intensity pattern associated with the Bessel beam of order m are determined by the positive critical points $\tilde{\rho}_{ml}$ of the Bessel function $J_m(\tilde{\rho})$, (the $\tilde{\rho}_{ml}$ denotes the $l-th$ critical point of J_m).

Now using Eqs. (2.36), (2.37) and (2.41) another direct computation shows that the curves and the caustics are given by

$$\tilde{\rho}^2 = \left(\mathcal{C} - m\beta - \frac{3m\pi}{2}\right)^2 + (m + \mathcal{L})^2, \tag{2.43}$$

and

$$\tilde{\rho}_c^2 \;=\; \tilde{x}_c^2 + \tilde{y}_c^2 = (m + \mathcal{L})^2. \tag{2.44}$$

respectively.

The wavefronts associated with the Bessel beam of order m are given by Eq. (2.43) with $\mathcal{L} = 0$, and the caustic associated with this family of wavefronts, that is, the geometrical caustic is a circle of radius m/k_t given by Eq. (2.44) with $\mathcal{L} = 0$. Thus, for the Bessel beam of order zero, the geometrical caustic on the plane is a point that coincides with the origin of coordinates. On the other hand, the maximum of the intensity pattern of the Bessel beam of order zero is given by $\tilde{\rho} = 0$. Therefore, for this particular case, the geometrical caustic *coincides* with the absolute maximum of the intensity pattern. However, for $m \neq 0$ the geometrical caustic does not coincide with the absolute maximum of the corresponding intensity pattern. To clarify this point in figure 2.5(a) we present the intensity pattern of the Bessel beam of order zero and the geometrical caustic, which is a single point (Red) in this case the caustic coincides with the absolute maximum. While in figure 2.5(b) we present the intensity pattern for a Bessel beam of order 3, the corresponding geometrical caustic (Red circle) and the absolute maximum (Purple circle), in this plot it is clear that the caustic does not coincide with absolute maximum of the intensity pattern. In fact one can show that in general the absolute maximum of the intensity pattern of a Bessel beam of order $m \neq 0$ does not coincide with the corresponding geometrical caustic, which is a circle of radius m/k_t.

In this work we use the intensity pattern of the Bessel beam of order m to determine the discrete values, $\mathcal{L}_{ml}$, of the parameter $\mathcal{L}$, such that the family of caustics coincide with the maxima of the pattern of the Bessel beam of order m. Therefore:

$$\mathcal{L}_{ml} \equiv \tilde{\rho}_{ml} - m, \tag{2.45}$$

where m is the order and l denotes the maxima of the intensity pattern of the Bessel beam. Thus, from Eq. (2.43)-(2.45) we have that the curves and caustics determined by the maxima of the intensity pattern of the Bessel beam of order m are given by

$$\tilde{\rho}^2 = \left(\mathcal{C} - m\beta - \frac{3m\pi}{2}\right)^2 + \tilde{\rho}_{ml}^2. \tag{2.46}$$

and

$$\tilde{\rho}_c^2 \;=\; \tilde{x}_c^2 + \tilde{y}_c^2 = \tilde{\rho}_{ml}^2. \tag{2.47}$$

respectively.

For $m = 0$, the curves are circles with radii $\sqrt{\mathcal{C}^2 + \tilde{\rho}_{0l}^2}$ and for $m \neq 0$ the curves are deformations of circles. The geometrical wavefronts are given by Eq. (2.46) with $\tilde{\rho}_{0l} = 0$. In Figure 2.6(a) we present some wavefronts (Blue) and the geometrical caustic (Red point) for the Bessel beam of order zero. In Figures 2.6(b) and 2.6(c) we present some curves (Blue) and the corresponding caustics (Red) determined by the first two maxima of the intensity pattern of the Bessel beam of order zero. In Figures 2.6(d)-2.6(f) we present the curves (Blue) and the corresponding caustics (Red) determined by the first three maxima of the intensity pattern of the Bessel beam of order 3.

From Eqs. (2.38), (2.39), (2.41) and (2.45) we have that the two-dimensional surfaces and caustics associated with the Bessel beam of order m are given by

$$\begin{aligned} \tilde{\rho}^2 &= (\mathcal{C} - m\beta - \frac{3m\pi}{2} - \tilde{z})^2 + \tilde{\rho}_{ml}^2, \\ \tilde{z} &= \tilde{z}, \end{aligned} \tag{2.48}$$

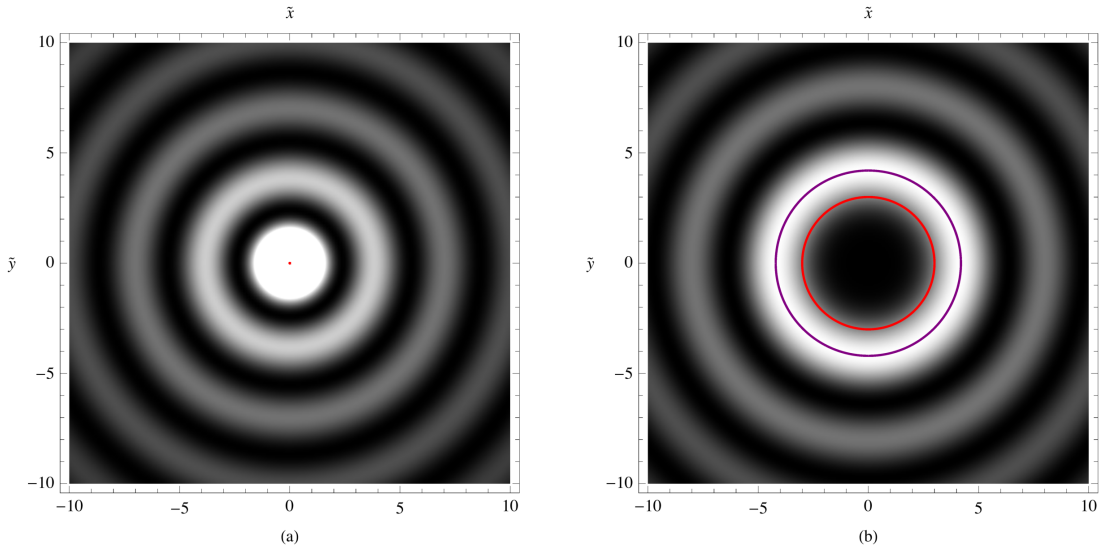

Figure 2.5: Here we present (a) part of the intensity pattern of the Bessel beam of order zero given by $[J_0(\tilde{\rho})]^2$ (GrayLevel) and the geometrical caustic (Red) given by (2.44) with $m = 0$ and $\mathcal{L} = 0$. (b) part of the intensity pattern of the Bessel beam of order 3 given by $[J_3(\tilde{\rho})]^2$ (GrayLevel) and the geometrical caustic a circle (Red) and the absolute maximum of the intensity pattern another circle (Purple). The geometrical caustic is given by (2.44) with $m = 3$ and $\mathcal{L} = 0$. In this plot it is clear that the geometrical caustic (Red circle) does not coincide with the absolute maximum of the intensity pattern (Purple circle).

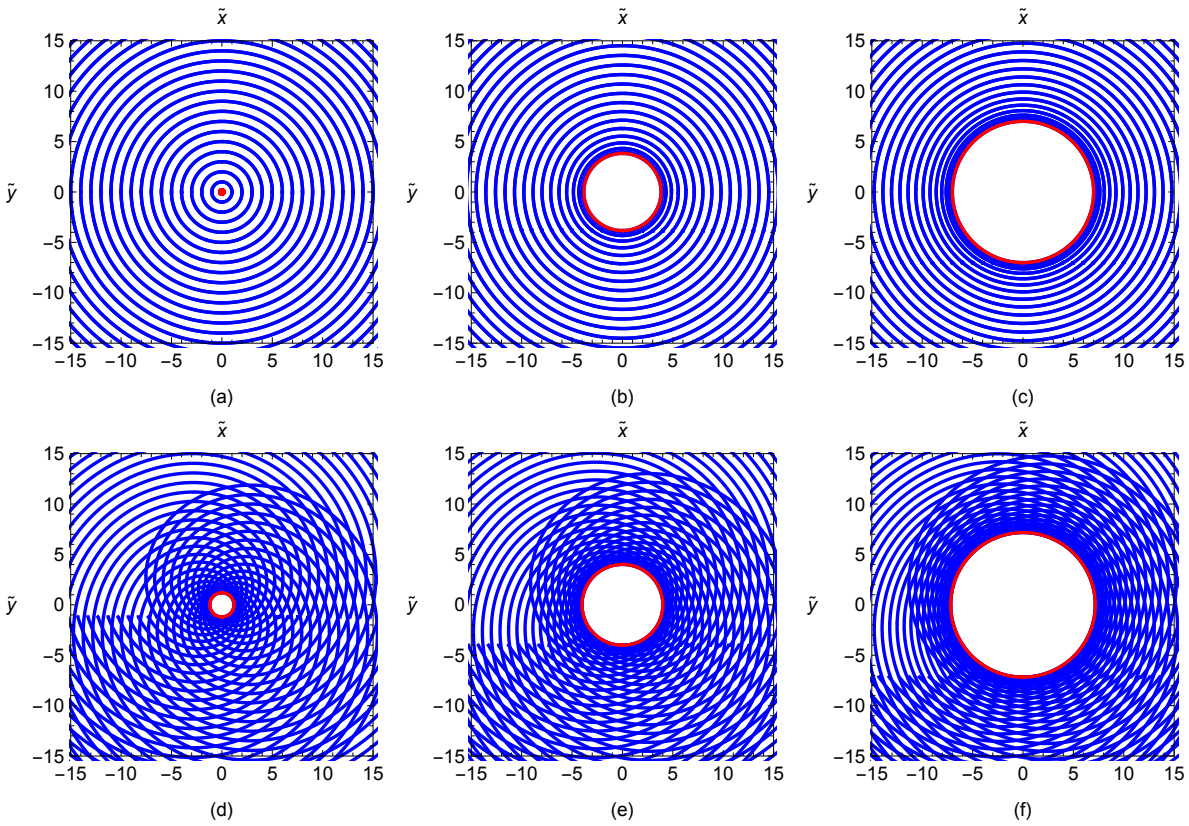

Figure 2.6: *Some one-dimensional curves given by Eq. (2.46) with* $\mathcal{C} = [-30, 30]$ *(Blue) and the corresponding caustics given by Eq. (2.47) (Red) for the cases: a)* $\mathcal{L}_{00} = 0.00$ *(some wavefronts (Blue) and the geometrical caustic (Red)), b)* $\mathcal{L}_{01} = 3.83$*, c)* $\mathcal{L}_{02} = 7.01$*, d)* $\mathcal{L}_{30} = 4.20$*, e)* $\mathcal{L}_{31} = 7.01$ *and f)* $\mathcal{L}_{32} = 10.17$*.*

and

$$\begin{aligned} \tilde{\rho}_c^2 &= \tilde{\rho}_{ml}^2. \\ \tilde{z} &= \tilde{z}, \end{aligned} \tag{2.49}$$

respectively.

From Eqs. (2.48) we have that the two surfaces given by $\mathcal{C} = 0$ and $\mathcal{C} = \mathcal{C}_0$ can be written in the following manner $\tilde{\rho}^2 = (-m\beta - \frac{3m\pi}{2} - \tilde{z}_1)^2 + \tilde{\rho}_{ml}^2$ and $\tilde{\rho}^2 = (\mathcal{C}_0 - m\beta - \frac{3m\pi}{2} - \tilde{z}_2)^2 + \tilde{\rho}_{ml}^2$, respectively; here $\tilde{z}_1$ and $\tilde{z}_2$ take values on the real line. Observe that taking $\tilde{z}_1 = \tilde{z}_2 - \mathcal{C}_0$ the second surface can be obtained from the first one. That is, any surface given by Eqs. (2.48) with $\mathcal{C} = \mathcal{C}_0$ is exactly the same as that given by Eqs. (2.48) with $\mathcal{C} = 0$. Therefore, the surfaces and caustics are invariant under translations along the Z axis. When $m = 0$ and $\tilde{\rho}_{0l} = 0$ the geometrical wavefronts associated with the Bessel beam of order zero are cones with apex at $\tilde{z} = \mathcal{C}$ and the geometrical caustic is a line that coincides with the Z axis, see Figure 2.7(a). On the other hand, for $m = 0$ and $\tilde{\rho}_{0l} \neq 0$ the two dimensional surfaces are hyperboloids of one sheet and the caustics are cylinders, see Figures 2.7(b) and 2.7(c). Finally, for $m \neq 0$, $\tilde{\rho}_{ml} \neq 0$ the two dimensional surfaces are deformations of hyperboloids of one sheet and the caustics are cylinders too, see Figures 2.7(d)-2.7(f) for the Bessel beam of order 3.

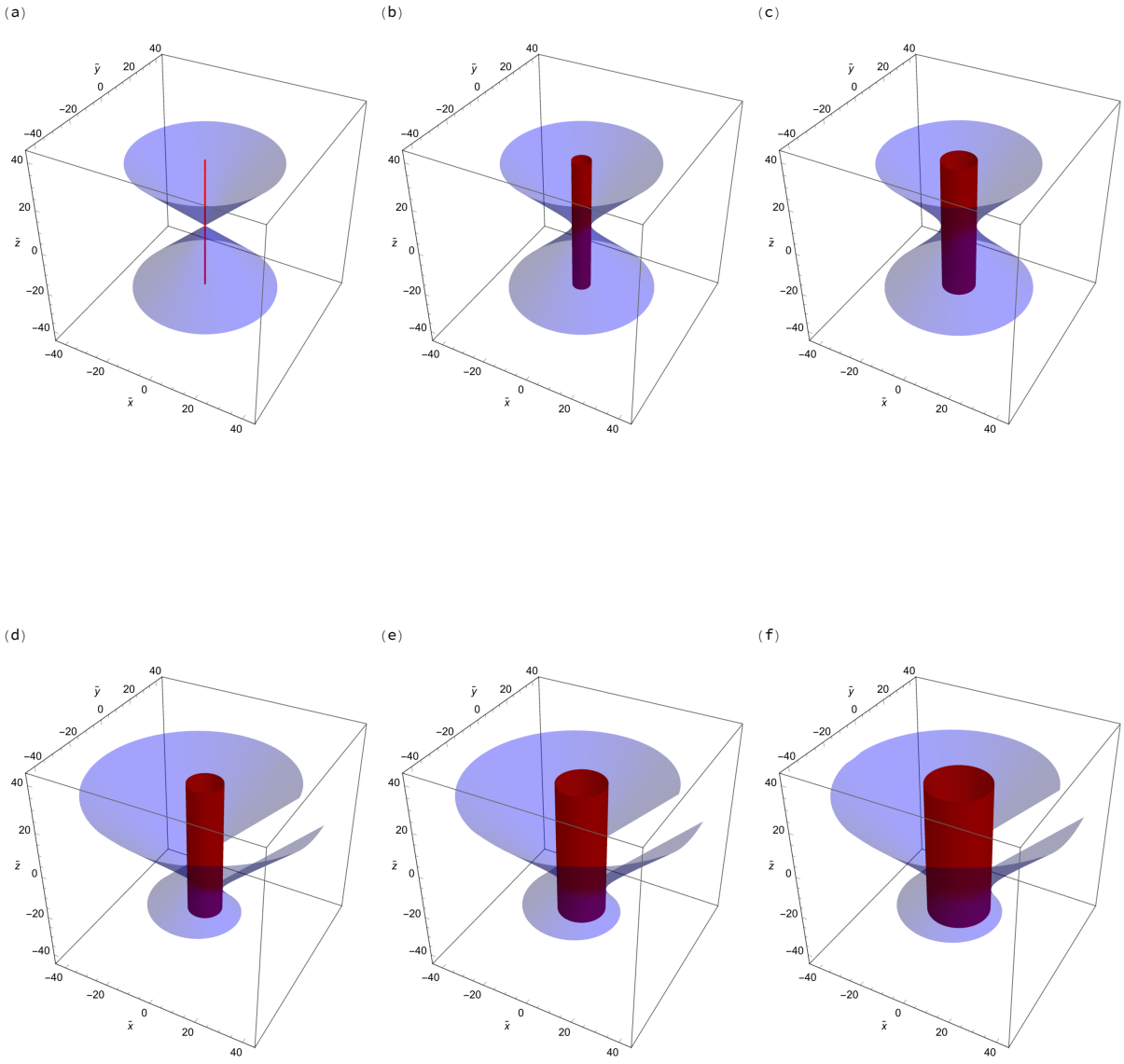

Figure 2.7: *Some two-dimensional surfaces given by Eqs. (2.48) with* $\mathcal{C} = 0$ *(Blue) and the corresponding caustics given by Eqs. (2.49) (Red) for the cases: a)* $\mathcal{L}_{00} = 0.00$ *(the wavefront (Blue) and the geometrical caustic (Red)), b)* $\mathcal{L}_{01} = 3.83$*, c)* $\mathcal{L}_{02} = 7.01$*, d)* $\mathcal{L}_{30} = 4.20$*, e)* $\mathcal{L}_{31} = 7.01$ *and f)* $\mathcal{L}_{32} = 10.17$*. Observe that the surfaces with* $\mathcal{L} \neq 0$*, which are not wavefronts, are smooth surfaces at the caustic regions.*

Chapter 3

Geometric treatment of the radiation captured by the Large Millimeter Telescope (LMT/GTM)

The most ambitious experimental project of our time, the Event Horizon Telescope (EHT) [34, 35], has set itself the task of studying in the most detailed possible way the rotating black hole that is hosted in the center of the galaxy M87 and the one hosted in the center of our Milky Way galaxy, and even generate the first real images of these objects. The results of this project will yield to new confirmations on the theory of Einstein's Relativity and therefore new questions and rethinkings about those hypotheses that we believed understanding. As a consequence, the black hole of our galaxy has been studied arduously in the last decade in a theoretical way. To do so, it is usually modeled as a black hole of Kerr type, that is to say, it is rotating about its axis of symmetry. The rotation affects the spacetime and therefore the radiation surrounding it, deflecting and phase-modifying it. Numerical studies of this dynamics suggest that the rotation generates a relativistic effect that imprints orbital angular momentum on such light in a process called Gravitational Faraday effect [6]. Tamburini et al. [6], calculated the integration of the null geodesic equations of light from orbiting point-like sources in the Kerr black hole equatorial plane to an asymptotic observer, and they were able to identify the phase change, the wavefront warping and to predict the associated light-beam orbital angular momentum spectra from linearly polarized to undergo polarization radiation.

Since in the Schwarzschild spacetime a part of the caustic associated with the light cone of a point light source is a semi-infinite straight line along the optical axis [36], then, asymptotically the wave describing the radiation of that point light source in the vicinity of the Schwarzschild black hole could be the zero-order Bessel beam. For this reason, in the present chapter, we assume that the radiation emitted by any point light source in the vicinity of a Kerr black hole is described asymptotically by a nonzero order Bessel beam, which gets its orbital angular moment from the rotation of the Kerr black hole. Our major goal is to compute the intensity pattern associated with the reflection of a Bessel beam of order m by the Event Horizon Telescope, in order to determine among other things, the rotation parameter of a Kerr black hole. As a first step, the aim of the present chapter is twofold; first we compute the reflection of an inclined plane wave by the LMT/GTM; and this is so because the LMT/GTM is the most important component of the EHT array and an inclined plane wave is the basic component of a Bessel beam of order m, that is; we compute the reflected wavefronts, light rays and caustic. The second aim is to compute the ronchigram for the reflection of the inclined plane wave, when the ronchigrating is placed for

example, at the caustic region.

The originality of the work developed in this chapter lies in the possibility of recognizing dynamic characteristics of the source by using the ronchigram obtained from a geometrical optics point of view. That is, we suppose that there is a source emitting radiation somewhere in the observable universe and, being very far away, it can be considered as a pointlike source; consequently the received radiation is a plane wavefront arriving with a certain inclination to the antenna. From the radiation collected by the antenna at the focal region, an experimental ronchigram can be generated and by comparing it with the theoretical one which is computed here, we could determine if the emitting source can be considered as static or not.

It is important to remark that the results presented here can be used for any parabolical mirror. However, for our numerical examples, we use the characteristic parameters of the LMT/GTM antenna.

3.1 Geometric optics of the reflection phenomenon by a parabolic mirror considering inclined incident light rays

In order to be as clear as possible, in this section we describe the procedure to compute the reflected light rays, wavefronts, marginal surfaces, their associated caustic and the ronchigram when the incident light rays strike the mirror with a certain inclination. In the general case the caustic is a two dimensional surface which locally has a stable singularity of the hyperbolic umbilic type[37, 40, 41]. These general results are applied for the antenna of the LMT/GTM. Since the Large Millimeter Telescope (LMT/GTM) is a revolution paraboloid with curvature radius $a = 35\,m$, external diameter $D_e = 50\,m$ and internal diameter $D_i = 3.5\,m$, then using cylindrical coordinates (ρ, ϕ, z), we describe it with the following equation

$$\begin{aligned} \mathbf{r}(\rho,\phi) &= \rho\hat{\rho}_\phi + \frac{\rho^2}{2a}\,\hat{z}, && (3.1)\\ \hat{\rho}_\phi &\equiv \cos\phi\,\hat{x} + \sin\phi\,\hat{y}, && (3.2) \end{aligned}$$

where $\frac{D_i}{2} \leq \rho \leq \frac{D_e}{2}$ and $0 \leq \phi < 2\pi$.

Using the (ρ, ϕ) coordinates which parametrize the points on the revolution paraboloid given by Eq. (3.1), a direct computation shows that the points on the inclined reference plane wavefront with normal vector

$$\begin{aligned} \hat{\mathbf{I}} &= -(\sin\alpha\hat{\rho}_\beta + \cos\alpha\hat{z}), && (3.3)\\ \hat{\rho}_\beta &\equiv \cos\beta\,\hat{x} + \sin\beta\,\hat{y}, && (3.4) \end{aligned}$$

where the inclination of the reference plane is specified by the angles α and β, and passing through the point $(0, 0, a)$, are given by the points of the space with vector position given by

$$\begin{aligned} \mathbf{r}_p &= \rho\cos^2\alpha\hat{\rho}_\phi - \rho\sin^2\alpha\sin(\beta-\phi)\hat{\phi}_\beta + \frac{(2a^2-\rho^2)\sin 2\alpha}{4a}\hat{\rho}_\beta\\ &+ \frac{2a^2+\rho^2+(2a^2-\rho^2)\cos 2\alpha - 2a\rho\cos(\beta-\phi)\sin 2\alpha}{4a}\hat{z}, && (3.5)\\ \hat{\phi}_\beta &\equiv -\sin\beta\,\hat{x} + \cos\beta\,\hat{y}, && (3.6) \end{aligned}$$

see Fig. (3.1). Therefore, using Eqs. (3.1) and (3.5) the incident light rays, $\mathbf{X}_I = \mathbf{r}_p + \sigma(\mathbf{r} - \mathbf{r}_p)$ can

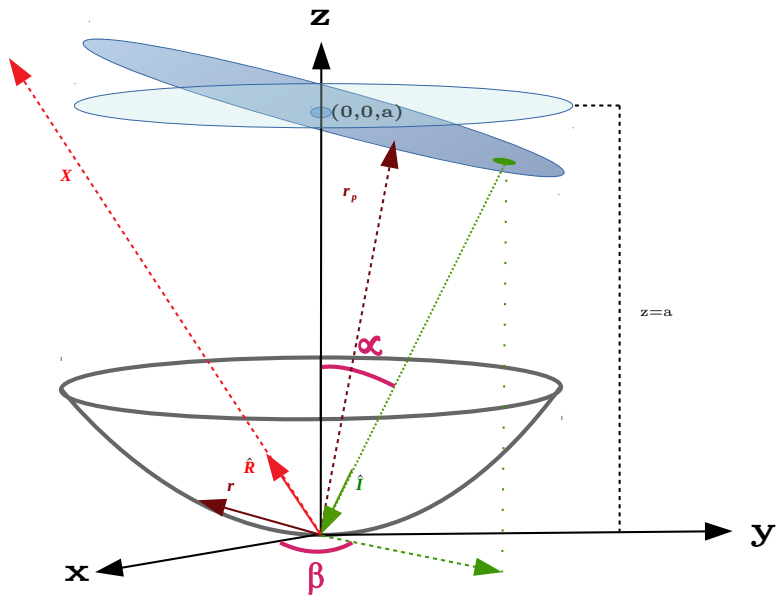

Figure 3.1: In this figure we show: the reference inclined plane (in blue), an incident light ray (in green), the corresponding reflected light ray (in red) and all the vectors and angles taking place in the problem.

be written in the following manner

$$\begin{aligned}\mathbf{X}_I = \quad & \frac{1}{4a}\{4a\rho[\sigma+(1-\sigma)\cos^2\alpha]\hat{\rho}_\phi+(1-\sigma)(2a^2-\rho^2)\sin 2\alpha\hat{\rho}_\beta \\ & -(1-\sigma)4a\rho\sin^2\alpha\sin(\beta-\phi)\hat{\phi}_\beta+[2a^2(1-\sigma)+\rho^2(1+\sigma) \\ & +(1-\sigma)[(2a^2-\rho^2)\cos 2\alpha-2a\rho\cos(\beta-\phi)\sin 2\alpha]\hat{z}\},\end{aligned} \tag{3.7}$$

where $0\leq\sigma\leq 1$ is a parameter labeling the points on the incident light ray from $\mathbf{r}_p$ to $\mathbf{r}$. Since the inclined incident plane wavefronts are given by $\mathbf{W}_I=\mathbf{r}_p+C_I\hat{\mathbf{I}}$, with $0\leq C_I\leq \max\mid\mathbf{r}-\mathbf{r}_p\mid$, then, using Eqs. (3.3) and (3.5) another direct computation shows that

$$\begin{aligned}\mathbf{W}_I &= \rho\cos^2\alpha\hat{\rho}_\phi-\rho\sin^2\alpha\sin(\beta-\phi)\hat{\phi}_\beta+\frac{(2a^2-\rho^2)\sin 2\alpha-4aC_I\sin\alpha}{4a}\hat{\rho}_\beta \\ &+ \frac{2a^2+\rho^2+(2a^2-\rho^2)\cos 2\alpha-2a\rho\cos(\beta-\phi)\sin 2\alpha-4aC_I\cos\alpha}{4a}\hat{z}.\end{aligned} \tag{3.8}$$

The two marginal surfaces associated with the incident light rays are given by Eq. (3.7) with $\rho=3.5/2\,m$ and $\rho=25\,m$ respectively. In Fig. 3.2 (a) we present the inclined reference plane for $\beta=0$ and $\alpha=\pi/10$ (in blue), some incident wavefronts (in light blue), the external and internal marginal surfaces of the incident light rays (in green) and the antenna (in gray).Observe that in the particular case $\alpha=0$, $\hat{\mathbf{I}}=-\hat{z}$, the reference plane, the incident light rays and the incident plane wavefronts take the following simple expressions

$$\mathbf{r}_p = \rho\hat{\rho}_\phi+a\,\hat{z}, \tag{3.9}$$

$$\mathbf{X}_I = \rho\hat{\rho}_\phi+\left[a(1-\sigma)+\frac{\sigma\rho^2}{2a}\right]\hat{z}, \tag{3.10}$$

$$\mathbf{W}_I = \rho\hat{\rho}_\phi+(a-C_I)\hat{z}, \tag{3.11}$$

respectively.

3.1.1 Reflected light rays

The reflected light rays are described by

$$\mathbf{X}_R = \mathbf{r} + \tau\hat{\mathbf{R}}, \tag{3.12}$$

τ is the distance from the point on the paraboloid, where an incident light ray strikes the mirror, with position vector $\mathbf{r}$ to an arbitrary point $\mathbf{X}_R$, on the reflected light ray which evolves in the direction $\hat{\mathbf{R}}$ given by the reflection law [42]

$$\hat{\mathbf{R}} = \hat{\mathbf{I}} - 2(\hat{\mathbf{I}}\cdot\hat{\mathbf{N}})\hat{\mathbf{N}}, \tag{3.13}$$

$$\hat{\mathbf{N}} = \frac{-\rho\hat{\rho}_\phi + a\hat{z}}{\sqrt{\rho^2+a^2}}, \tag{3.14}$$

is the unit normal vector to the parabolical antenna. Therefore using Eqs. (3.3), (3.13), and (3.14), a direct computation shows that

$$\hat{\mathbf{R}} = \frac{[-a\cos\alpha + \rho\cos(\beta-\phi)\sin\alpha](2\rho\hat{\rho}_\phi + 2a\hat{z})}{a^2+\rho^2} - (\sin\alpha\hat{\rho}_\beta + \cos\alpha\hat{z}). \tag{3.15}$$

Thus, using Eqs. (3.1), (3.12) and (3.15) we obtain that the corresponding reflected light rays can be written in the following manner

$$\begin{aligned}\mathbf{X}_R = \quad & \rho\hat{\rho}_\phi + \frac{\rho^2}{2a}\hat{z} - \frac{2\tau[a\cos\alpha - \rho\cos(\beta-\phi)\sin\alpha](\rho\hat{\rho}_\phi + a\hat{z})]}{a^2+\rho^2} \\ & -\tau(\sin\alpha\hat{\rho}_\beta + \cos\alpha\hat{z}).\end{aligned} \tag{3.16}$$

Now we will use a parameterization of the reflected light rays that is more convenient for the calculation of the ronchigram. For this purpose, we equate the z component of the position vector of the points of the reflected light rays with a new variable that we denote by z_0. The new parametrization in z_0 terms is

$$\begin{aligned}\mathbf{X}_R = \quad & \frac{1}{\lambda}2a^2(a-2z_0)\rho\cos\alpha\hat{\rho}_\phi - \sin\alpha[a^2(2az_0+\rho^2)\hat{\rho}_\beta \\ & +\rho^2(2a(a-z_0)+\rho^2)(\cos\beta\hat{\rho}_{2\phi} - \sin\beta\hat{\phi}_{2\phi})] \\ & +z_0\,\hat{z},\end{aligned} \tag{3.17}$$

where $\lambda = 2a[(a^2-\rho^2)\cos\alpha - 2a\rho\cos(\beta-\phi)\sin\alpha]$ and $\rho^2/2a \le z_0 < \infty$. Since the reflected wavefronts are given by $\mathbf{W}_R = \mathbf{r} + [C_R - |\mathbf{r}-\mathbf{r_p}|]\hat{\mathbf{R}}$, then using Eqs. (3.1), (3.5) and (3.15), another direct computation shows that the corresponding reflected wavefronts can be written in the following manner

$$\mathbf{W}_R = \rho\hat{\rho}_\phi + \frac{\rho^2}{2a}\hat{z} + [C_R - |\,\mathbf{r}-\mathbf{r}_p\,|][\delta\rho\hat{\rho}_\phi + (\delta a - \cos\alpha)\hat{z} - \sin\alpha\hat{\rho}_\beta], \tag{3.18}$$

where $\delta = 2[(-a\cos\alpha + \rho\cos(\beta-\phi)\sin\alpha)/(\rho^2+a^2)]$ and $C_R \ge \max|\,\mathbf{r}-\mathbf{r}_p\,|$. The two marginal surfaces associated with the reflected light rays are given by Eq. (3.17) with $\rho = 3.5/2\,m$ and $\rho = 25\,m$ respectively. In Fig. 3.2 (b) we present some representative reflected wavefronts (in light blue), the external and internal marginal surfaces of the reflected light rays (in red) and the antenna (in gray). In Fig. 3.2 (c) we present four representative reflected wavefronts (in light blue) and the antenna (in gray).

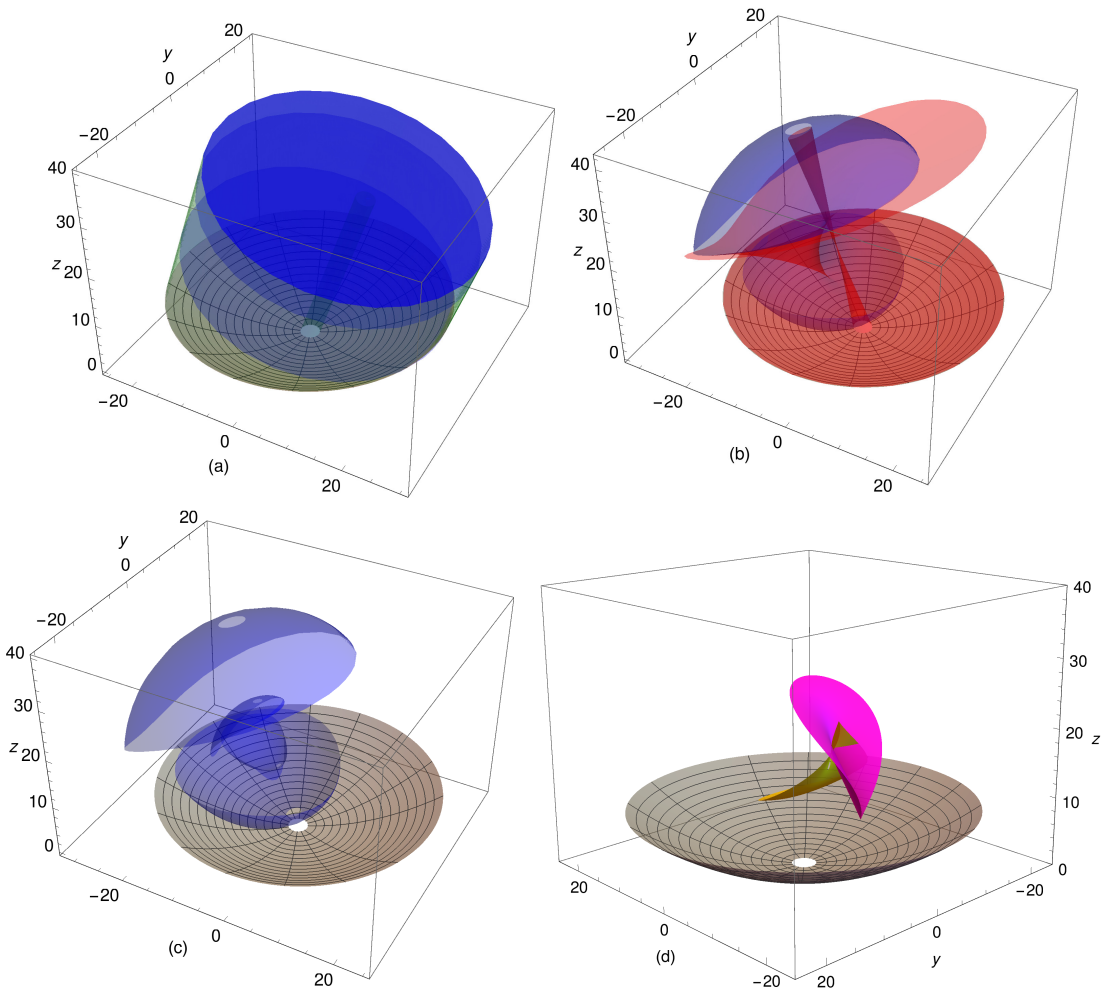

Figure 3.2: In this plot we show: (a) the inclined reference plane for $\beta = 0$ and $\alpha = \pi/10$ (in blue), some incident wavefronts (in light blue), the external and internal marginal surfaces of the incident light rays (in green) and the antenna (in gray). (b) Some representative reflected wavefronts (in light blue), the external and internal marginal surfaces of the reflected light rays (in red) and the antenna (in gray). (c) Four representative reflected wavefronts (in light blue) and the antenna (in gray). (d) The two branches of the caustic (in magenta and yellow) and the antenna (in gray).

3.1.2 The caustic

Observe that the reflected light rays and wavefronts are described by maps between two subsets of $\mathcal{R}^3$. Therefore, their corresponding critical and caustics sets associated with those maps will be computed using the definition given in chapter one.
In the present case, a direct computation shows that the critical set associated with the map in Eq. (3.16), which describes the reflected light rays, is obtained from the following condition

$$J_{\mathbf{X}_R} = \left(\frac{\partial \mathbf{X}_R}{\partial \rho}\right) \cdot \left[\left(\frac{\partial \mathbf{X}_R}{\partial \phi}\right) \times \left(\frac{\partial \mathbf{X}_R}{\partial \tau}\right)\right] = H_2\tau^2 + H_1\tau + H_0 = 0, \tag{3.19}$$

where

$$H_2 = \hat{\mathbf{R}} \cdot \left(\frac{\partial \hat{\mathbf{R}}}{\partial \rho} \times \frac{\partial \hat{\mathbf{R}}}{\partial \phi}\right), \tag{3.20}$$

$$H_1 = \hat{\mathbf{R}} \cdot \left(\frac{\partial \mathbf{r}}{\partial \rho} \times \frac{\partial \hat{\mathbf{R}}}{\partial \phi} - \frac{\partial \mathbf{r}}{\partial \phi} \times \frac{\partial \hat{\mathbf{R}}}{\partial \rho}\right), \tag{3.21}$$

$$H_0 = \hat{\mathbf{R}} \cdot \left(\frac{\partial \mathbf{r}}{\partial \rho} \times \frac{\partial \mathbf{r}}{\partial \phi}\right). \tag{3.22}$$

Due to in general $H_2 \neq 0$, the critical set has two branches given by

$$\tau_{\pm} = \frac{-H_1 \pm \sqrt{H_1^2 - 4H_2H_0}}{2H_2}. \tag{3.23}$$

Therefore the caustic set of the reflected light rays given by Eq. (3.16) can be written in the following manner

$$\mathbf{X}_{c_{\pm}} = \mathbf{r} + \left(\frac{-H_1 \pm \sqrt{H_1^2 - 4H_2H_0}}{2H_2}\right)\hat{\mathbf{R}}. \tag{3.24}$$

To obtain the critical and caustic sets of the map in Eq. (3.17) where we use as an independent variable to z_0 we proceed as follows. We know that $z_0 = \rho^2/2a + \tau(\hat{\mathbf{R}} \cdot \hat{z})$, therefore the critical set of the map in Eq. (3.17) can be written in the following manner

$$z_{0_{\pm}} = \frac{\rho^2}{2a} + \left(\frac{-H_1 \pm \sqrt{H_1^2 - 4H_2H_0}}{2H_2}\right)\hat{\mathbf{R}} \cdot \hat{z}, \tag{3.25}$$

and the caustic set is also given by Eq. (3.24). For the case $\alpha = 0$, Eq. (3.25) reduces to $z_{0_{\pm}} = a/2$ meanwhile the caustic set or caustic given by Eq. (3.24) reduces to $\mathbf{X}_c = (a/2)\hat{z}$, which coincides with the focal point of the parabolical antenna.

In Fig. 3.2 (d) we present the parabolical antenna and the two branches of the caustic, in Fig. 3.3 (a) we present the two branches of the caustic and two particular reflected wavefronts and finally in Fig. 3.3 (b) we can see that the caustic has a singularity of the hyperbolic umbilic type; all this figures are for the case $\beta = 0$, $\alpha = \pi/10$ and taking the parameters of the antenna (LMT/GTM). Furthermore, since we are interested in computing the ronchigram, we have to study the distribution of the reflected light rays on planes $z = constant$ around the caustic region. Therefore in Fig. (3.4) we present the intersection between some reflected light rays with the planes $z_0 = 15\,m$, $z_0 = 17.5\,m$ (the focus) and $z_0 = 20\,m$ for the antenna of the LMT/GTM with $\beta = 0$ and $\alpha = \pi/200$. From Fig. 3.3 (b) it is clear that the dominant aberration of the optical system for these parameters is that of the coma one. In Fig. (3.5), we present similar results for the case $\beta = 0$ and $\alpha = \pi/10$.

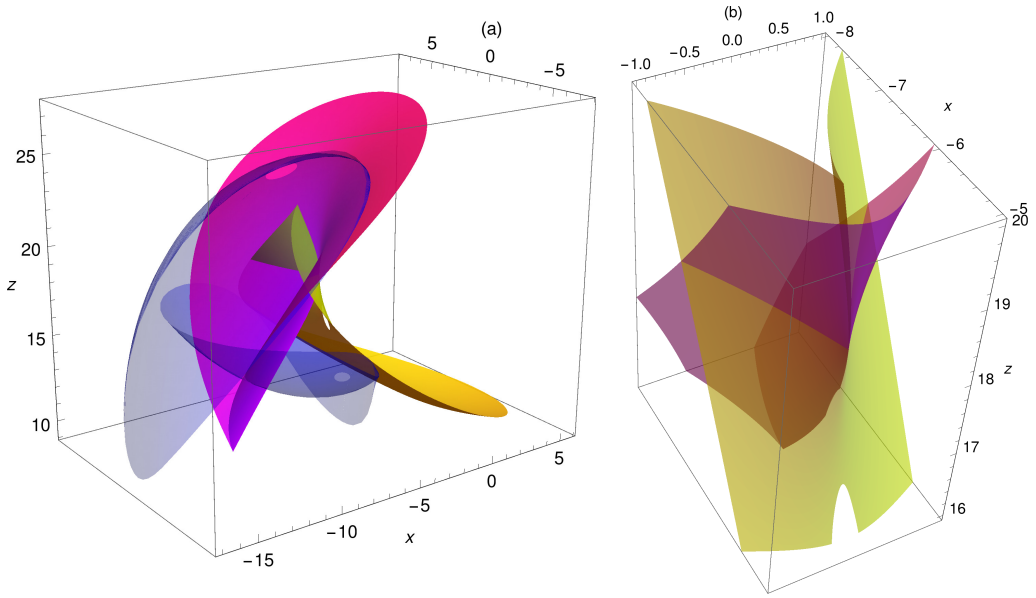

Figure 3.3: In this plot we show: (a) the two branches of the caustic (for the value z_0^+ in magenta and for the value z_0^- in yellow) and some reflected wavefronts (in light blue); (b) the zoom to the caustics for the intersection zone where the stable singularities can be indentified.

It is important to remark that a lengthy but direct computation shows that the caustic for this problem has a singularity of hyperbolic umbilic type, because under a change of coordinates, $\rho = \rho(s_1, s_2)$, $\phi = \phi(s_1, s_2)$, $X = X(C_1, C_2, C_3)$, $Y = Y(C_1, C_2, C_3)$ and $Z = Z(C_1, C_2, C_3)$, it can be transformed into the canonical form of the hyperbolic umbilic caustic given by $C_{1\pm} = 3s_1^2 \mp 6s_2\sqrt{s_1 s_2}$, $C_{2\pm} = 3s_2^2 \mp 6s_1\sqrt{s_1 s_2}$ and $C_{3\pm} = \pm 6\sqrt{s_1 s_2}$. Furthermore, another direct computation shows that working up to third order in ρ/a and to first order in α, the aberration or deformation on the reflected wavefront is given by

$$\begin{aligned} \Delta\Phi &= -\left(\frac{\alpha}{a^2}\right)\rho^3\cos\phi \\ &= -\left(\frac{\alpha}{a^2}\right)(x^2+y^2)x, \end{aligned} \tag{3.26}$$

which corresponds to the aberration of coma.

3.1.3 The ronchigram

In this subsection we compute the ronchigram associated with the reflected light rays by the parabolical antenna when the ronchigrating is placed at a plane $z = z_0$ with its rulling bands parallel to the x axis. To this end, we introduce a new coordinate system (T_x, T_y, T_z) with origin at the point $(0, 0, z_0)$. Then, we compute the region filled out by the reflected light rays, in particular, we determine this region at the plane where the ronchigrating is placed. Finally, we compute the ronchigram when the grating is placed before, at and after the focus of the parabolical antenna.

In order to compute the ronchigram, on the (T_x, T_y) plane of the new coordinate system we place a ronchigrating with rulling bands given by

$$\mathbf{T}_G = x_G\,\hat{x} + nd\,\hat{y} + z_0\,\hat{z}, \tag{3.27}$$

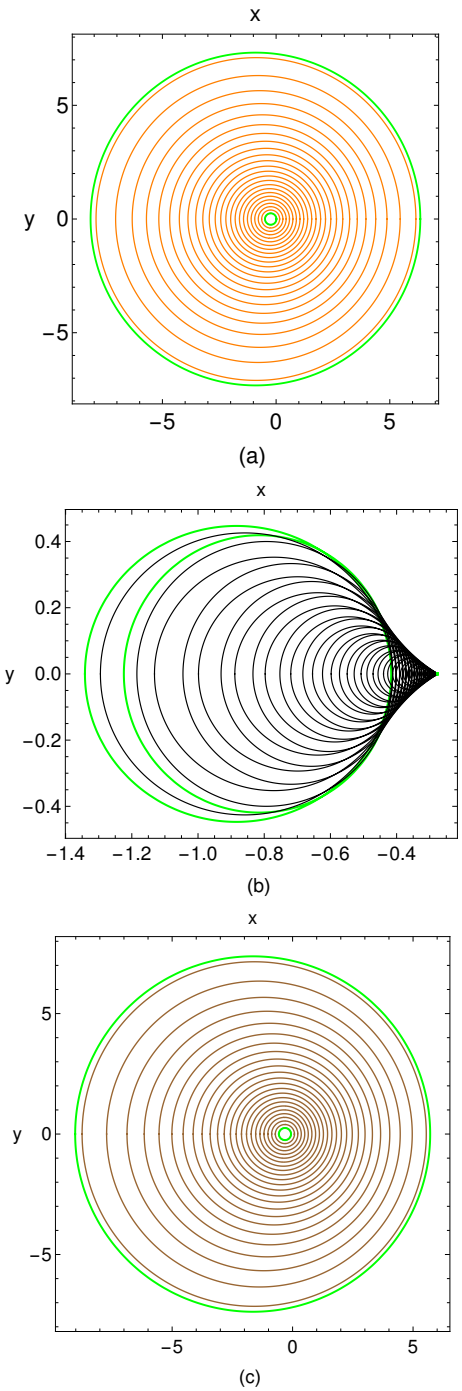

Figure 3.4: In this plot we show the intersections of some reflected light rays with the planes (a) $z_0 = 15\,m$, (b) $z_0 = 17.5\,m$ (focal plane of the parabolical antenna) and (c) $z_0 = 20\,m$ for $\beta = 0$ and $\alpha = \pi/200$. The green color curves correspond to the intersections of the marginal surfaces.

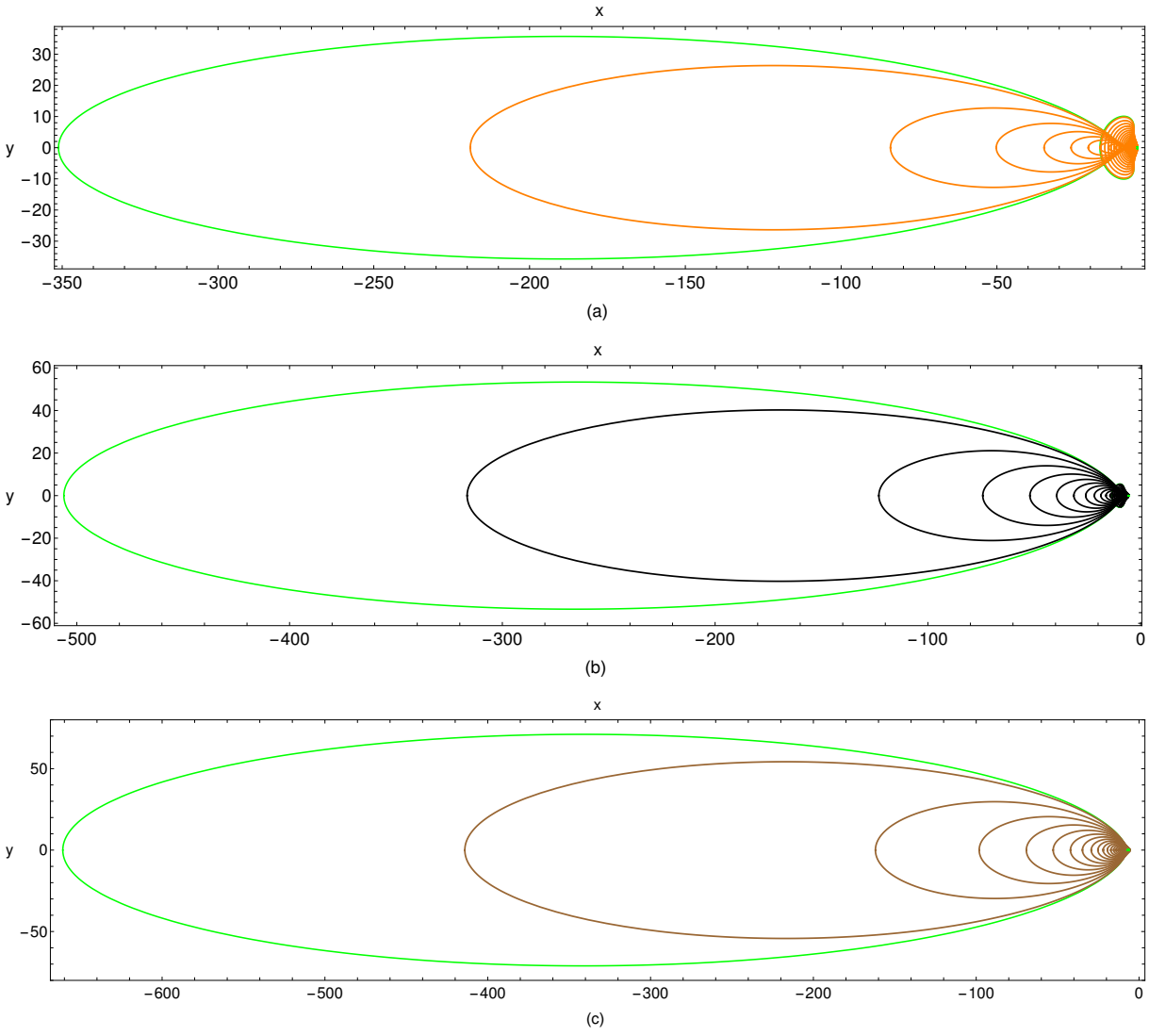

Figure 3.5: In this plot we show the intersections of some reflected light rays with the planes (a) $z_0 = 15\,m$, (b) $z_0 = 17.5\,m$ (focal plane of the parabolical antenna) and (c) $z_0 = 20\,m$ for $\beta = 0$ and $\alpha = \pi/10$. The green color curves correspond to the intersections of the marginal surfaces.

where $n = 0, \pm 1, \pm 2, ...$, x_G is a parameter labeling the points on a particular rulling band, its domain is determined by the internal and external marginal surfaces, and d is the separation between the rulling bands. Then we look for all the points on the mirror $(\rho_s, \phi_s, \rho_s^2/2a)$, such that ρ_s and ϕ_s are solutions to the following equation

$$\mathbf{X}_R = \mathbf{T}_G. \tag{3.28}$$

Using Eqs. (3.27) and (3.17) a direct computation shows that the condition (3.28) can be written in the following manner

$$F(\rho, \phi, z_0, \alpha, \beta) = x_G\, w(\rho, \phi, \alpha, \beta), \tag{3.29}$$
$$G(\rho, \phi, z_0, \alpha, \beta) = nd\, w(\rho, \phi, \alpha, \beta), \tag{3.30}$$

where

$$\begin{aligned} F &= 2a^2(a - 2z_0)\rho\cos\alpha\cos\phi \\ &- \{a^2(2az_0 + \rho^2)\cos\beta + \rho^2[2a(a - z_0) + \rho^2]\cos(\beta - 2\phi)\}\sin\alpha, \qquad (3.31) \\ G &= \sin\alpha\{-a^2(2az_0 + \rho^2)\sin\beta + \rho^2[2a(a - z_0) + \rho^2]\sin(\beta - 2\phi)\} \\ &+ 2a^2(a - 2z_0)\rho\cos\alpha\sin\phi, \qquad (3.32) \\ w &= 2a[(a^2 - \rho^2)\cos\alpha - 2a\rho\cos(\beta - \phi)\sin\alpha]. \qquad (3.33) \end{aligned}$$

Here we assume that the known parameters are (α, β), which give the direction of the incident plane wavefront, a which gives the antenna radio's curvature and (x_G, nd, z_0) which give the information of the points of the ronchigrating. Thus, from Eqs. (3.29)-(3.33), we find that the solutions to the Eqs. (3.29) and (3.30) can be written in the following way

$$\rho_s = \rho(\alpha, \beta, a, x_G, nd, z_0), \tag{3.34}$$
$$\phi_s = \rho(\alpha, \beta, a, x_G, nd, z_0). \tag{3.35}$$

To compute the ronchigram at the plane $z = z_1 > z_0$, we proceed as follow; first in Eq. (3.17) which describes the reflected light rays, we replace the parameter z_0 by z_1, that is $\mathbf{X}_R = \mathbf{X}_R(\alpha, \beta, a, \rho, \phi, z_1)$. Finally, in this last resulting equation we replace ρ by ρ_s and ϕ by ϕ_s. Therefore, the ronchigram at the plane z_1 is given by

$$\mathbf{S} = \mathbf{X}_R(\alpha, \beta, a, \rho_s, \phi_s, z_1). \tag{3.36}$$

In this work, we present plots of the projection of the ronchigram at the plane $z = 0$ given by

$$S_x = \rho_s\cos\phi_s, \tag{3.37}$$
$$S_y = \rho_s\sin\phi_s, \tag{3.38}$$

for different positions of the ronchigrating for the case $\alpha = \pi/10$. In Fig. (3.6) we present the two branches of the caustic and the planes $z_0 = 9\,m, 15\,m, 17.5\,m, 20\,m$ and $28\,m$. On these planes, we place the ronchigrating for the LMT/GTM parabolical antenna to compute the corresponding projections of the ronchigrams on the plane $z = 0$. The planes $z_0 = 9\,m$ and $z_0 = 28\,m$ are out of the caustic region while the planes $z_0 = 15\,m, 17.5\,m$ and $20\,m$ intersect the caustic region. In Fig. (3.7) we show the projections of the ronchigrams at plane $z = 0$ for the case $\beta = 0$ and $\alpha = \pi/200$, and the ronchigrating is placed at the planes: (a) $z_0 = 9\,m$, (b) $z_0 = 15\,m$, (c) $z_0 = 17.5\,m$, (d) $z_0 = 20\,m$, (e) $z_0 = 23\,m$ and (f) $z_0 = 28\,m$. Finally in Fig.(3.8) we present similar results for the projection of the ronchigram for the case $\beta = 0$ and $\alpha = \pi/10$.

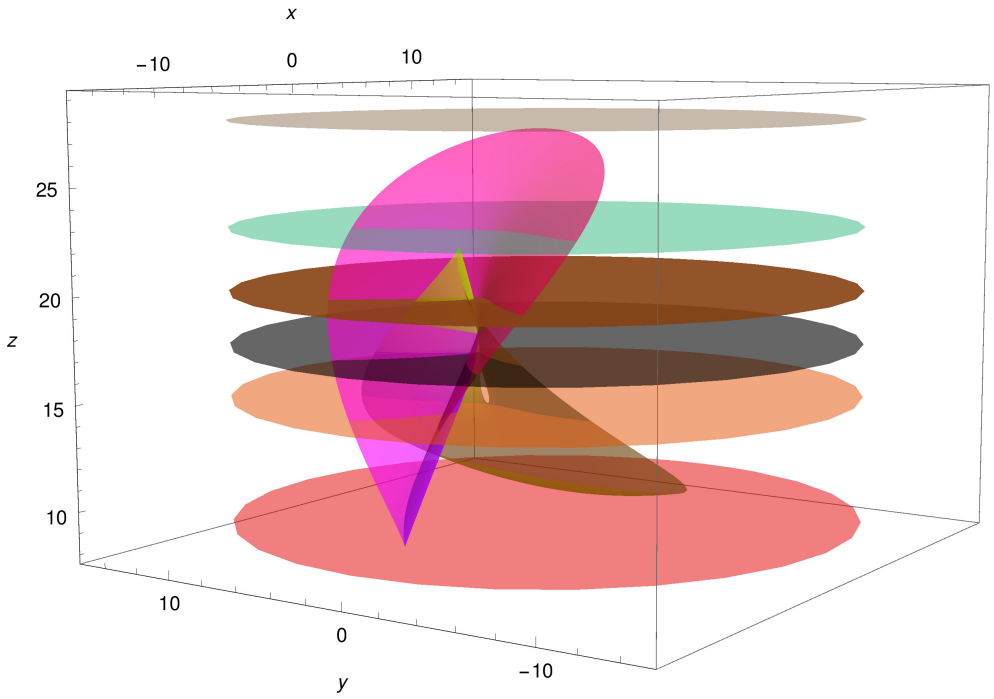

Figure 3.6: In this plot we present the two branches of the caustic and some parts of the planes $z_0 = 9\,m$ (in light red), $15\,m$ (in light orange), $17.5\,m$ (in light black), $20\,m$ (in brown), $23\,m$ (in cyan) and $28\,m$ (in gray), where we place the ronchigrating to compute the corresponding projections of the ronchigrams at the plane $z = 0$.

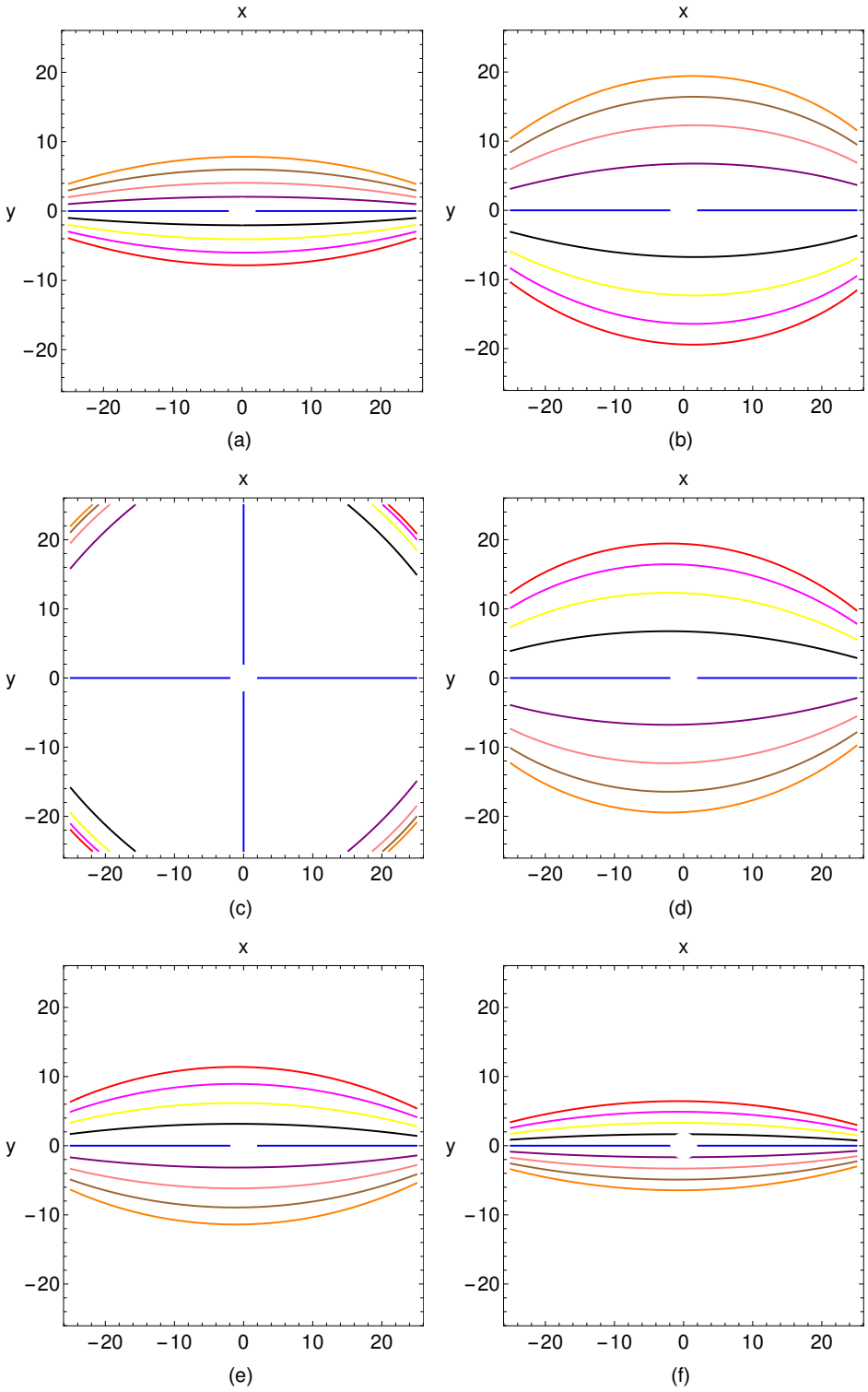

Figure 3.7: In this plot we show the projections of the ronchigrams at plane $z = 0$ for the case $\beta = 0$ and $\alpha = \pi/200$, and the ronchigrating is placed at the planes: (a) $z_0 = 9\,m$, (b) $z_0 = 15\,m$, (c) $z_0 = 17.5\,m$, (d) $z_0 = 20\,m$, (e) $z_0 = 23\,m$ and (f) $z_0 = 28\,m$.

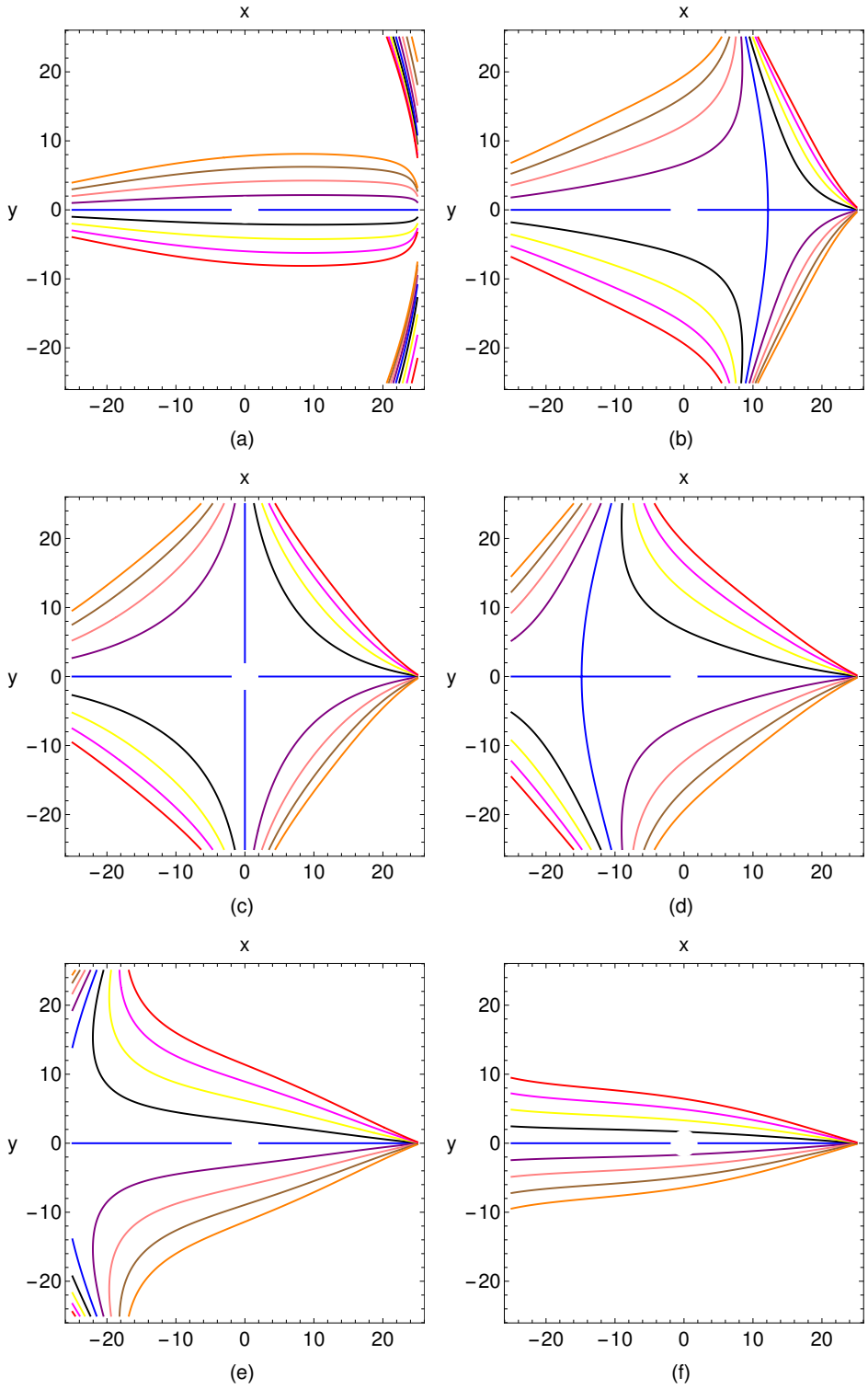

Figure 3.8: In this plot we show the projections of the ronchigrams at plane $z = 0$ for the case $\beta = 0$, $\alpha = \pi/10$ and the ronchigrating is placed at the planes: (a) $z_0 = 9\,m$, (b) $z_0 = 15\,m$, (c) $z_0 = 17.5\,m$, (d) $z_0 = 20\,m$, (e) $z_0 = 23\,m$ and (f) $z_0 = 28\,m$.

Chapter 4

Towards the detection of radiation emitted by a light source in the vicinity of a Kerr BH

Remember that the main motivation of our project is to develop an optical procedure to detect the radiation from point light sources affected by astrophysical rotating objects, which generates a gravitational field described by the Kerr solution. The hypothesis of the work is based on the fact that for the Schwarzschild spacetime a part of the caustic associated with the light cone of a point light source is a semi-infinite straight line along the optical axis [11], then, asymptotically the wave describing the radiation of that point light source in the vicinity of the Schwarzschild black hole could be the zero-order Bessel beam. On the other hand, we assume that the radiation emitted by any point light source in the vicinity of a Kerr black hole is described asymptotically by a nonzero order Bessel beam, which gets its orbital angular moment from the rotation of the Kerr black hole. Under that assumption, our major goal in this chapter is to compute an expression for the intensity pattern associated with the reflection of a Bessel beam of order m by the LMT/GTM.

To this end, we first present the Kirchhoff's diffraction theory applied to the phenomenon of reflection of light rays by a parabolic mirror, in particular that of the LMT/GTM antenna. Then, we assume that the Bessel beam of order m is the superposition of many planewaves as many points are on a circle, using this information we obtain an expression for the scalar optical field associated with the reflection of a Bessel beam of order m by the LMT/GTM antenna. On the certain appoximations, we finally obtain an expression for the intensity pattern of that reflected radiation.

4.1 Derivation of the integral Kirchhoff's formula

In the diffraction Kirchhoff's scalar theory, one has an incident, scalar, monochromatic optical field solution to the scalar wave equation in free space that goes through an aperture, experiencing the so-called diffraction phenomena. Assuming that the diffracted scalar monochromatic optical field is another solution to the wave equation in free space, the aim of the scalar Kirchhoff's difraction theory, which is a valid approximation for small wavelengths compared with the dimension of the aperture, is to obtain an expression for the diffracted optical beam from the knowledge of the incident one. Here we present a derivation of the integral Kirrchoff's formula and we introduce the notation that will be used in this chapter. To this end, we consider two scalar monocromatic optical waves given by $V(x,y,z,t) = U(x,y,z)e^{-i\omega t}$ and $V'(x,y,z,t) = U'(x,y,z)e^{-i\omega t}$, which are

solutions to the scalar wave equation in free space. Therefore, U and U' satisfy the Helmholtz equation. That is,

$$(\nabla^2 + k^2)U = 0, \quad (\nabla^2 + k^2)U' = 0. \tag{4.1}$$

Now, we take a region of the free space with volume v bounded by a closed surface S. We assume that U and U' have continuous first and second order partial derivatives, within and on the surface. Furthermore, we define the following vector field

$$\mathbf{J} \equiv U\nabla U' - U'\nabla U. \tag{4.2}$$

Using Eqs. (4.1), a direct computation shows that

$$\nabla \cdot \mathbf{J} = U\nabla^2 U' - U'\nabla^2 U = 0, \tag{4.3}$$

$$\nabla \times \mathbf{J} = 2(\nabla U \times \nabla U'). \tag{4.4}$$

Therefore, from the Gauss's theorem in three dimensions, we obtain that

$$\int_S \mathbf{J} \cdot \hat{\mathbf{N}}\, dS = 0, \tag{4.5}$$

where $\hat{\mathbf{N}}$ is the unit normal vector to S, pointing inward to this surface. If $\mathbf{X} = X\hat{x} + Y\hat{y} + Z\hat{y}$ and $\mathbf{r} = x\hat{x} + y\hat{y} + z\hat{y}$ are the vector positions of two arbitrary points within S, then we define

$$\mathbf{R} \equiv \mathbf{X} - \mathbf{r} = R\,\hat{\mathbf{R}}. \tag{4.6}$$

In the Kirchhoff's theory one assumes that

$$U'(\mathbf{r}, \mathbf{X}) = \frac{e^{ikR}}{R}, \tag{4.7}$$

that is, this function depends on the two position vectors $\mathbf{r}$ and $\mathbf{X}$. It is important to remark that in Eq. (4.6), $\mathbf{X}$ is assumed to be consider as a constant vector, while the vector $\mathbf{r}$ is not a constant one. Therefore, U' is singular when $\mathbf{r} = \mathbf{X}$; that is, it is singular at $R = 0$. This means that the point within the surface S with vector position $\mathbf{X}$, must be removed from the integration domain. To this end, we enclose that point with a sphere of radius ϵ and center it at the point with vector position $\mathbf{X}$. Therefore, under this assumption the Eq. (4.5) transforms into the following equation

$$\int_S \mathbf{J} \cdot \hat{\mathbf{N}}\, dS + \int_{S'} \mathbf{J} \cdot \hat{\mathbf{N}}'\, dS' = 0, \tag{4.8}$$

where $\hat{\mathbf{N}}'$ is the unit normal vector to the spherical surface, see Fig. (4.1).

Using Eqs. (4.2), (4.6) and (4.7), a direct computation shows that

$$\begin{aligned} \mathbf{J} \cdot \hat{\mathbf{N}} &= \left[U\nabla\left(\frac{e^{ikR}}{R}\right) - \left(\frac{e^{ikR}}{R}\right)\nabla U\right] \cdot \hat{\mathbf{N}} \\ &= U\left[\frac{e^{ikR}}{R}\left(ik - \frac{1}{R}\right)\right][\hat{\mathbf{R}} \cdot \hat{\mathbf{N}}] - \left(\frac{e^{ikR}}{R}\right)\left[\hat{\mathbf{N}} \cdot \nabla U\right], \end{aligned} \tag{4.9}$$

and

$$\begin{aligned} \mathbf{J} \cdot \hat{\mathbf{N}}' &= \left[U\nabla\left(\frac{e^{ikR}}{R}\right) - \left(\frac{e^{ikR}}{R}\right)\nabla U\right] \cdot \hat{\mathbf{N}}' \\ &= U\left[\frac{e^{ikR}}{R}\left(ik - \frac{1}{R}\right)\right] - \left(\frac{e^{ikR}}{R}\right)\left[\hat{\mathbf{N}}' \cdot \nabla U\right]. \end{aligned} \tag{4.10}$$

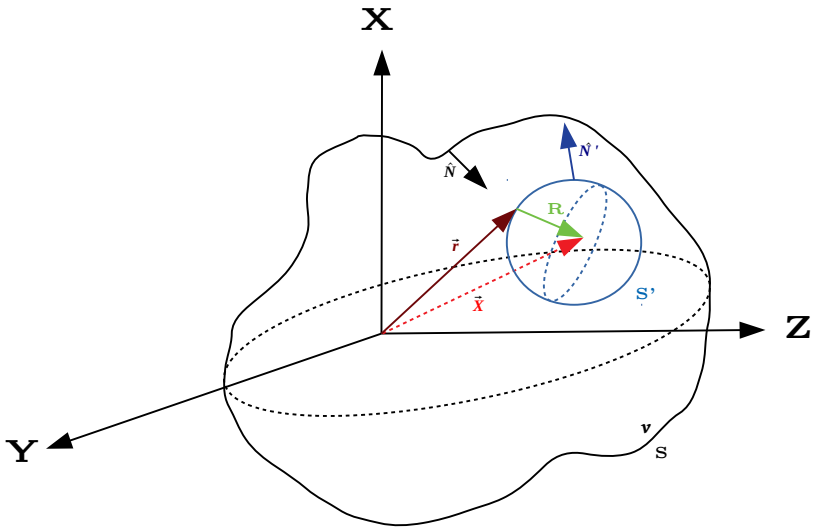

Figure 4.1: The general problem. Let a volume v bounded by a closed surface S, with $\mathbf{X}$ be any point within v.

To perform the integral on the spherical surface, we take $\mathbf{r} - \mathbf{X} = \epsilon \hat{\mathbf{N}}'(\theta', \phi')$, where θ' and ϕ' are coordinates on the spherical surface and $dS' = \epsilon^2 \sin\theta' d\theta' d\phi'$. Then

$$\int_{S'} \mathbf{J} \cdot \hat{\mathbf{N}}' \, dS' = \int_0^{\pi} \int_0^{2\pi} \left\{ U \left[\frac{e^{ik\epsilon}}{\epsilon} \left(ik - \frac{1}{\epsilon} \right) \right] - \left(\frac{e^{ik\epsilon}}{\epsilon} \right) \left[\hat{\mathbf{N}}' \cdot \nabla U \right] \right\} \epsilon^2 \sin\theta' d\theta' d\phi'. \tag{4.11}$$

Therefore,

$$\lim_{\epsilon \to 0} \int_{S'} \mathbf{J} \cdot \hat{\mathbf{N}}' \, dS' \quad = \quad - \int_0^{\pi} \int_0^{2\pi} U(\mathbf{X}) \sin\theta' d\phi' = -4\pi U(\mathbf{X}). \tag{4.12}$$

Finally, from Eqs. (4.8) and (4.12) we obtain what it is known as the Helmholtz and Kirchhoff integral's theorem [47]:

$$U(\mathbf{X}) = \frac{1}{4\pi} \int_S \left\{ U \left[\frac{e^{ikR}}{R} \left(ik - \frac{1}{R} \right) \right] (\hat{\mathbf{R}} \cdot \hat{\mathbf{N}}) - \left(\frac{e^{ikR}}{R} \right) (\hat{\mathbf{N}} \cdot \nabla U) \right\} dS. \tag{4.13}$$

Before continuing, it is important to remark that Eq. (4.13) establishes that the function $U(\mathbf{X})$ evaluated at a point, with vector position $\mathbf{X}$, inside the surface S is given in terms of the same function U and ∇U evaluated at the point on the surface S. In other words, if we know U and ∇U on the surface S, then Eq. (4.13) allow us to determine the function U at any point inside the surface S.

4.1.1 Kirchhoff boundary conditions

Remember that in the Kirchhoff's diffraction theory we have an incident scalar optical field, U^i, which is diffracted by a given aperture on a opaque screen. To apply the Eq. (4.13) to determine the diffracted scalar optical field, Kirchhoff assumed that the surface S is constituted by three surfaces:

A, the aperture, B and C the unlit sides of the screen. The Kirchhoff's boundary conditions on these surfaces are as follow:

$$\begin{aligned} \text{on } A: U &= U^i;\ \nabla U = \nabla U^i, \\ \text{on } B: U &= 0;\quad \nabla U = 0, \\ \text{on } C: U &= 0;\quad \nabla U = 0. \end{aligned} \tag{4.14}$$

Therefore, using Eqs. (4.13), (4.14) and assuming that $k \gg 1/R$, the diffracted scalar optical field can be written in the following manner

$$U(\mathbf{X}) = \frac{1}{4\pi}\int_A \frac{e^{ikR}}{R}\left\{ik(\hat{\mathbf{R}}\cdot\hat{\mathbf{N}})U^i - (\hat{\mathbf{N}}\cdot\nabla U^i)\right\}dS. \tag{4.15}$$

In the special case when the incident scalar optical field is a spherical wave, emitted by a point light source with vector position $\mathbf{r}_p$, then

$$U^i = \frac{\Lambda e^{ikI}}{I},\ \ \nabla U^i\cdot\hat{\mathbf{N}} = \frac{\Lambda e^{ikI}}{I}\left[ik - \frac{1}{I}\right]\cos(\hat{\mathbf{N}},\hat{I}), \tag{4.16}$$

where Λ is a constant and

$$\mathbf{I} \equiv \mathbf{r} - \mathbf{r}_p = I\,\hat{\mathbf{I}}. \tag{4.17}$$

Therefore, on the assumption that, $k \gg 1/I$ from Eqs. (4.15) and (4.16) we finally obtain

$$U(\mathbf{X}) \approx \frac{-i\Lambda}{2\lambda}\int_A \frac{e^{ik(I+R)}}{IR}[\cos(\hat{N},\hat{I}) - \cos(\hat{N},\hat{R})]dS. \tag{4.18}$$

Eq.(4.18) is known as the Fresnel-Kirchhoff diffraction formula, and is the expresion which help us to find the field at point $\mathbf{X}$, in an approximate form, considering the conditions listed throughout this development.

4.2 The intensity pattern associated with the reflection of a Bessel beam of order m by the LMT/GTM antenna

Since the ideal Bessel beam of order m is the superposition of many plane waves as many points are on a circle, with constant amplitude Λ, a phase given by $k[\hat{\mathbf{X}}_I\cdot\hat{\mathbf{I}} + m\beta]$, and since we are interested only in the reflection of all the light rays of this plane wave by the parabolical antenna of the LMT/GTM, it is neccesary to parametrize the phase of this plane wave by using the coordinates labeling the points on the parabolical antenna. To this end, we assume that the reference plane wavefront associated with this plane wave is given by the vector position $\mathbf{r}_p$ obtained in the previous chapter. Therefore, to compute the reflection of a Bessel beam of order m we first compute the reflected scalar optical field assuming that the incoming radiation is such that

$$U^i = \Lambda e^{ik[I+\frac{m\beta}{k}]},\ \ \nabla U^i\cdot\hat{\mathbf{N}} = ik\Lambda e^{ik[I+\frac{m\beta}{k}]}\cos(\hat{\mathbf{N}},\hat{\mathbf{I}}), \tag{4.19}$$

where

$$\mathbf{I} \equiv \mathbf{r} - \mathbf{r}_p = I\,\hat{\mathbf{I}}. \tag{4.20}$$

Therefore, from Eqs. (4.15) and (4.19) we obtain

$$U(\mathbf{X}) = \frac{-i\Lambda}{2\lambda}\int_A \frac{e^{ik(I+R+\frac{m\beta}{k})}}{R}[\cos(\hat{\mathbf{N}},\hat{\mathbf{I}}) - \cos(\hat{\mathbf{N}},\hat{\mathbf{R}})]dS. \tag{4.21}$$

Observe that this Eq. (4.21) can be written in the following manner

$$U(\mathbf{X}) = \frac{i\Lambda}{2\lambda}\int_A \frac{e^{ik\Phi}}{R}(\hat{\mathbf{R}}-\hat{\mathbf{I}})\cdot\hat{\mathbf{N}}dS, \tag{4.22}$$

$$\Phi = R + I + \frac{m\beta}{k} = (\mathbf{r}-\mathbf{r}_p)\cdot\hat{\mathbf{I}} + (\mathbf{X}-\mathbf{r})\cdot\hat{\mathbf{R}} + \frac{m\beta}{k}. \tag{4.23}$$

Now we use the reflection law, $\hat{\mathbf{R}}_G = \hat{\mathbf{I}} - 2(\hat{\mathbf{I}}\cdot\hat{\mathbf{N}})\hat{\mathbf{N}}$ to replace $(\hat{\mathbf{R}}-\hat{\mathbf{I}})\cdot\hat{\mathbf{N}}$ by $-2(\hat{\mathbf{I}}\cdot\hat{\mathbf{N}})$. Furthermore, in the denominator we replace R by Z. In this way, we obtain the following appoximation

$$U(\mathbf{X}) = -\frac{i\Lambda}{\lambda Z}\int_A (\hat{\mathbf{I}}\cdot\hat{\mathbf{N}})e^{ik\Phi}dS. \tag{4.24}$$

Since,

$$\hat{\mathbf{I}} = -(\sin\alpha\hat{\rho}_\beta + \cos\alpha\hat{z}), \tag{4.25}$$

$$\hat{\rho}_\beta \equiv \cos\beta\,\hat{x} + \sin\beta\,\hat{y}, \tag{4.26}$$

$$\hat{\mathbf{N}} = \frac{-\rho\hat{\rho}_\phi + a\hat{z}}{\sqrt{\rho^2+a^2}}, \tag{4.27}$$

$$\hat{\mathbf{I}}\cdot\hat{\mathbf{N}} = \frac{-a\cos\alpha + \rho\cos(\beta-\phi)\sin\alpha}{\sqrt{a^2+\rho^2}}, \tag{4.28}$$

$$dS = \frac{\rho}{a}\sqrt{\rho^2+a^2}\,d\rho d\phi. \tag{4.29}$$

Therefore,

$$U(\mathbf{X}) = \frac{i\Lambda}{\lambda a Z}\int_0^{2\pi}\int_{D_i/2}^{D_e/2}(a\cos\alpha - \rho\cos(\beta-\phi)\sin\alpha)\,e^{ik\Phi}\rho d\rho d\phi, \tag{4.30}$$

where

$$\Phi = \frac{(2a^2-\rho^2)\cos\alpha - 2a\rho\cos(\beta-\phi)\sin\alpha}{2a} + \sqrt{\tau^2+\rho^2+\frac{(\rho^2-2aZ)^2}{4a^2} - 2\rho\tau\cos(\theta-\phi)} + \frac{m\beta}{k} \tag{4.31}$$

which is valid for any value of α.

Now, we assume that $a\cos\alpha - \rho\cos(\beta-\phi)\sin\alpha$ is approximately a constant which we take it into account in the Λ constant. Furthermore, in the above expression for Φ we assume that $Z >> a$, $Z >> D_e/2$ and $Z >> \tau$, then, up to first order in τ from Eqs. (4.30) and (4.33) we obtain a physical-geometrical appoximation to the reflection of an incoming plane wave associated with the Bessel beam of order m given by

$$U(\mathbf{X}) = \frac{i\Lambda}{\lambda a Z}\int_0^{2\pi}\int_{3.5/2}^{25} e^{ik\Phi_{AP}}\rho d\rho d\phi, \tag{4.32}$$

where

$$\Phi_{AP} = Z + \frac{(2a^2-\rho^2)\cos\alpha - 2a\rho\cos(\beta-\phi)\sin\alpha - \rho^2}{2a} - \frac{\rho\tau\cos(\theta-\phi)}{Z} + \frac{m\beta}{k}. \tag{4.33}$$

Until now, we have obtained a physical-geometrical approximation (4.32) to the reflection by the parabolical antenna of the LMT/GTM, of a plane wavefront determined by a Bessel beam of

order m (4.19). Now, we consider the radiation associated with the Bessel beam of order m, that is, reflected by the LMT/GTM antenna, which is given by the superposition of the radiation (4.32) on the angle β. That is,

$$U(\mathbf{X}) = \frac{i\Lambda}{\lambda a Z}\int_0^{2\pi}\int_0^{2\pi}\int_{3.5/2}^{25} e^{ik\Phi_{AP}}\rho d\rho d\phi d\beta. \tag{4.34}$$

The integration on β and ϕ allows to write Eq. (4.34) in the following manner

$$U_B(\mathbf{X}) = -\frac{4\pi^2 i^{(1-2m)}\Lambda e^{i[k(Z+a\cos\alpha)-m\theta]}}{\lambda a Z}\int_{3.5/2}^{25}\rho e^{-ik[\frac{\rho^2}{2a}(\cos\alpha+1)]}J_m(k\rho\sin\alpha)J_m\left(\frac{k\rho\tau}{Z}\right)d\rho. \tag{4.35}$$

Finally, up to this appoximation the intensity pattern associated with the scalar optical field (4.35); that is, the intensity pattern associated with the reflection of a Bessel beam of order m by the LMT/GTM antenna, can be written in the following manner

$$I_B = \frac{16\pi^4\Lambda^2}{\lambda^2 a^2 Z^2}\left|\int_{3.5/2}^{25}\rho e^{-ik[\frac{\rho^2}{2a}(\cos\alpha+1)]}J_m(k\rho\sin\alpha)J_m\left(\frac{k\rho\tau}{Z}\right)d\rho\right|^2. \tag{4.36}$$

For the special case of an incident plane wave, that is, when $\alpha = 0$, $m = 0$ and $Z >> a-(\rho^2/a)$, then Eqs. (4.35) and (4.36) reduce to

$$U_{PW}(\mathbf{X}) = -\frac{2\pi i\Lambda e^{ikZ}}{a\tau}\left[\rho J_1\left(\frac{k\tau\rho}{Z}\right)\right]_{3.5/2}^{25}, \tag{4.37}$$

$$I_{PW} = \frac{4\pi^2\Lambda^2}{a^2\tau^2}\left|\left[\rho J_1\left(\frac{k\tau\rho}{Z}\right)\right]_{3.5/2}^{25}\right|^2. \tag{4.38}$$

To evaluate in numerical wave the integral in Eq. (4.36) we define the following variables: $\tilde{\rho} = k\rho$, $\tilde{\tau} = k\tau$, $\tilde{a} = ka$ and $\tilde{Z} = kZ$. In terms of these new variables Eqs. (4.36) and (4.38) take the following form

$$I_B = \frac{16\pi^4\Lambda^2}{\lambda^2\tilde{a}^2\tilde{Z}^2}\left|\int_{3.5k/2}^{25k}\tilde{\rho}e^{-i[\frac{\tilde{\rho}^2}{2\tilde{a}}(\cos\alpha+1)]}J_m(\tilde{\rho}\sin\alpha)J_m\left(\frac{\tilde{\rho}\tilde{\tau}}{\tilde{Z}}\right)d\tilde{\rho}\right|^2. \tag{4.39}$$

$$I_{PW} = \frac{4\pi^2\Lambda^2}{\tilde{a}^2\tilde{\tau}^2}\left|\left[\tilde{\rho}J_1\left(\frac{k\tilde{\tau}\tilde{\rho}}{\tilde{Z}}\right)\right]_{3.5k/2}^{25k}\right|^2. \tag{4.40}$$

It is impotant to remark that in this work we are assuming that in the asymptotic region of the Schwarzschild black hole the optical scalar field associated with the radiation of a point like source located near the event horizon is described by the zero order Bessel beam. For this reason in Figures 4.2-4.4 (a) we present the normalized intensity patterns associated with the Bessel beam of zero order when $\alpha = \pi/200$, $\alpha = \pi/100$ and $\alpha = \pi/10$ respectively. Furthermore, in this work we are also asuming that the optical scalar field associated with a point like source near of the event horizon of the black hole, in the asymptotic region is described by a Bessel beam of order $m \neq 0$. For this reason in Figures 4.2-4.4 we also present the normalized intensity patterns associated with the Bessel beams of order $m = 5$ and $m = 10$, when $\alpha = \pi/200$, $\alpha = \pi/100$ and $\alpha = \pi/10$ such that in: (b), (e), (h) $\tilde{Z} = 50$, and (c), (f), (i) $\tilde{Z} = 100$. These plots provide the behavior of the normalized intensity patterns of the reflection of the Bessel beams with $m = 0$, $m = 5$ and $m = 10$ by the LMT/GTM antenna.

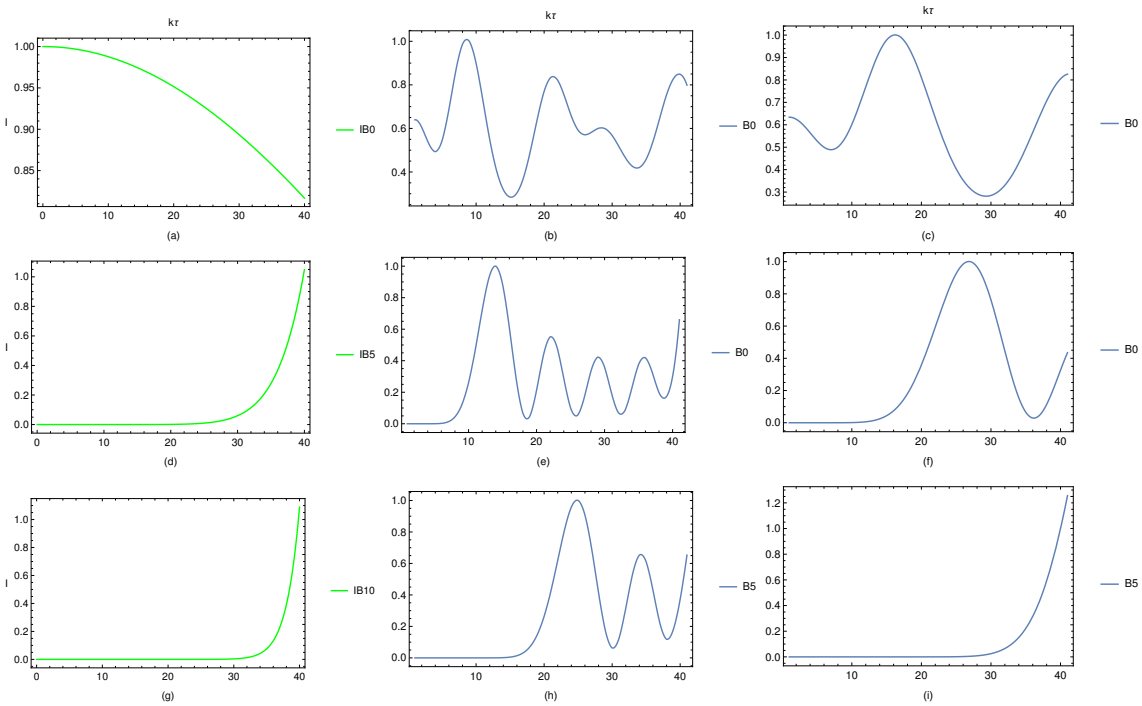

Figure 4.2: In this plot we show the normalized Intensity I for the incident ideal Bessel beam, and for the reflected Bessel beams, for different values of m, τ and $\alpha = \pi/200$, when (a):$m = 0$, (b):$m = 0$, $kZ = 50$, (c):$m = 0$, $kZ = 100$, (d):$m = 5$, (e):$m = 5$, $kZ = 50$, (f):$m = 5$, $kZ = 100$, (g):$m = 10$, (h):$m = 10$, $kZ = 50$ and (i):$m = 10$, $kZ = 100$.

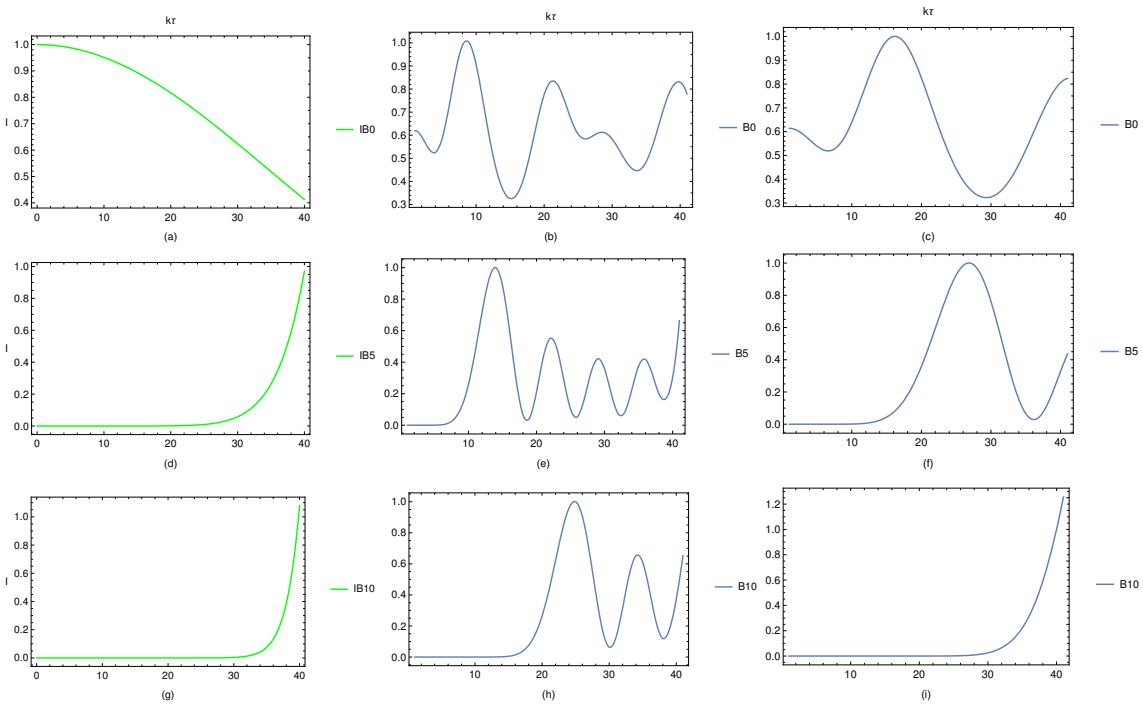

Figure 4.3: In this plot we show the normalized Intensity I for the incident ideal Bessel beam, and for the reflected Bessel beams, for different values of m, τ and $\alpha = \pi/100$, when (a):$m = 0$, (b):$m = 0$, $kZ = 50$, (c):$m = 0$, $kZ = 100$, (d):$m = 5$, (e):$m = 5$, $kZ = 50$, (f):$m = 5$, $kZ = 100$, (g):$m = 10$, (h):$m = 10$, $kZ = 50$ and (i):$m = 10$, $kZ = 100$.

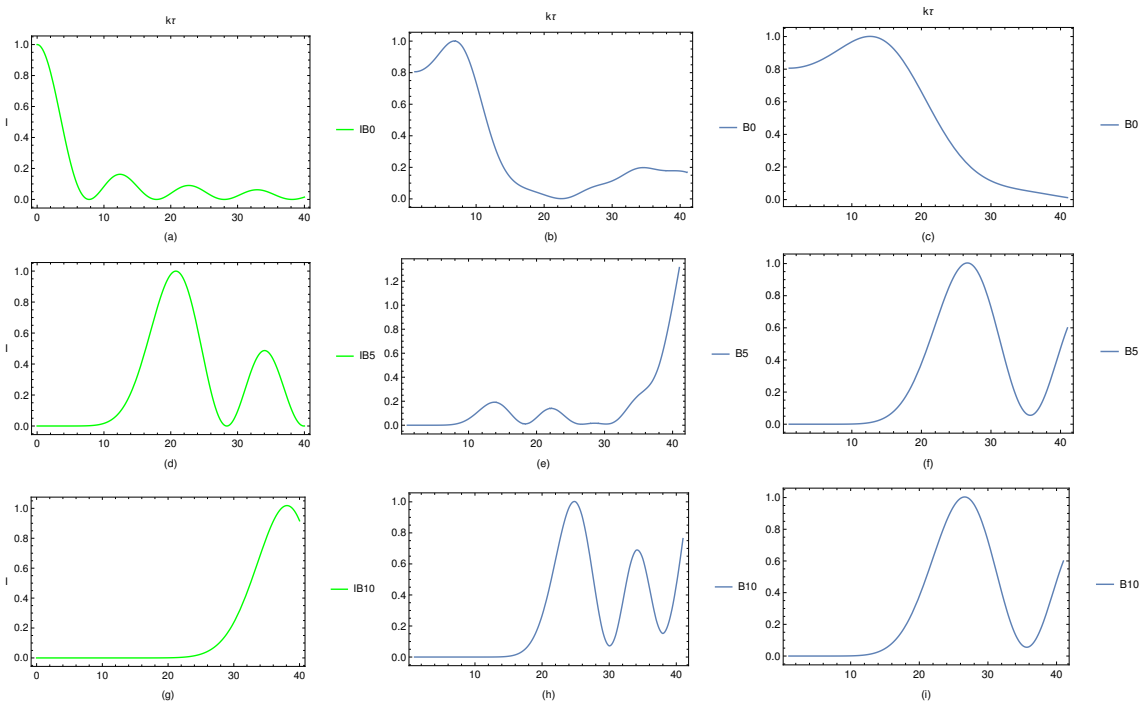

Figure 4.4: In this plot we show the normalized Intensity I for the incident ideal Bessel beam, and for the reflected Bessel beams, for different values of m, τ and $\alpha = \pi/10$, when (a):$m = 0$, (b):$m = 0$, $kZ = 50$, (c):$m = 0$, $kZ = 100$, (d):$m = 5$, (e):$m = 5$, $kZ = 50$, (f):$m = 5$, $kZ = 100$, (g):$m = 10$, (h):$m = 10$, $kZ = 50$ and (i):$m = 10$, $kZ = 100$.

Chapter 5

Discussion of results and future work

Along the work in chapter 2, we have shown that the intensity pattern of a nondiffracting beam is determined by an arbitrary positive real function $O(\beta)$ defined on the momentum or frequency space and a complete integral of both the eikonal and Laplace equations given by Eq. (2.22). Using those results we have associated a two-parameter family of one-dimensional curves and a one-parameter family of caustics on the plane to the intensity pattern given by Eqs. (2.36) and (2.37) respectively. Furthermore, we have presented the two-dimensional surfaces and caustics in the three space associated with the nondiffracting beam (2.19). We have found that in the case of the Bessel beam of order m the parameter characterizing the caustic family $\mathcal{L}$ can be chosen in such a way that the caustics coincide with the maxima of the intensity pattern. It is important to emphasize that for this particular example, the geometrical caustics do not determine the maxima of the intensity except the maximum of the Bessel beam of order zero. Since $O(\beta) = constant$ for a Bessel beam, then the intensity pattern is totally determined by the complete integral; that is, by the arbitrary real function $g(\beta)$. Therefore, we claim that the family of caustics (2.37) defined in this work will be determined by the maxima of the intensity pattern of a such nondiffracting beam. The results presented in this chapter, suggest to introduce a generalization of the geometrical caustic concept. That is, *to define the caustic associated with an arbitrary scalar optical field as the maxima of the corresponding intensity pattern*. We remark that in accordance with the results presented in reference [27], we believe that the parameter $\mathcal{L}$ could be related to the wavelength of the scalar optical field. Furthermore, we point out that our main interest in the geometrical characterization of a nondiffracting beam is to study the image formation problem [28] by using the wavefronts, curves and caustics determined by their maxima. In particular, we are interested in computing the ronchigram [29] associated with a Bessel beam of order m by using the wavefronts, curves and caustics determined in this work and compare it with the real one obtained from the experiment. We believe that by using a nondiffracting beam in the Ronchi test or in any other optical test one could obtain better results than those obtained by illuminating the optical system under test with plane or spherical waves. We remark that in the case of the Bessel beam the parameter $\mathcal{L}$ introduced in the present work can be chosen to determine any value of the intensity pattern associated with the Bessel beam of order m. This way, for example, by a suitable choice of $\mathcal{L}$ we can do that the caustic family coincides with the zeros of $|J_m(\tilde{\rho})|^2$. In this work we have chosen the parameter $\mathcal{L}$ to be determined by the maxima of the Bessel beam of order m because for this type of beam the geometrical caustic gives a *qualitative description of the absolute maximum of the intensity pattern* and because we believe that the caustics determined by the maxima of the intensity pattern will give a better accuracy in the image formation problem than the geometrical ones.

As we have remarked in the introduction, an optical field is a solution of the Maxwell equations. Therefore, to study the properties such as the quality of any optical system, one must use the Maxwell theory. However, if the polarization effects are no important, it is common to use the

scalar wave theory to test the quality of the optical systems. Even more, to design optical systems such as telescopes and microscopes, it is enough to use the geometrical optics approximation. It is important to remark that from the Maxwell equations or from the scalar wave equation under the assumption that the wavelength of the corresponding field goes to zero one obtains the eikonal equation in an isotropic optical medium. That is, in the geometrical optics approximation, any optical field solution to the Maxwell equations and any scalar wave field solution of the scalar wave equation is characterized by a particular family of wavefronts, light rays and in general a caustic region. Therefore, to give a theoretical description of any optical test we have to our disposition: the Maxwell theory, the scalar wave theory and the geometrical optics approximation. In this work, we have restricted our attention to the scalar nondiffacting beams, which are exact solutions of the scalar wave equation in free space. In particular, we have shown that in the case of the scalar wave Bessel beams it is possible to give a generalization of the geometrical caustic. That is, this generalization is defining a family of caustics determined by all the maxima, absolute and relative ones, of the intensity pattern of the scalar Bessel beam of order m.

It is important to remark that any nondiffacting beam introduced by Durnin has a dependence of the form $e^{i(k_z z-\omega t)}$, is determined by a positive real function $O(\beta)$ and a one parameter family of solutions of both the eikonal and Laplace equations in free space [1]. One can show that there is a subset of optical fields solutions to the Maxwell equations in free space determined by the same one parameter family of solutions of the eikonal and Laplace equations in free space, which can be consider as the vectorial Durnin nondiffacting beams [30]. That subset contains as a particular member the optical Bessel beam, which has been the object of several studies [31, 32, 33]. It is well known that the intensity pattern associated with an optical Bessel beam, solution to the Maxwell equations in free space, is different from that determined by the corresponding scalar wave Bessel beam because the polarization effects play a major role. Therefore, we suggest that *in the case of the optical Bessel beam one could define a family of caustics as determined by all the maxima of the corresponding intensity.* Thus as we have shown in chapter two in the case of the scalar Bessel beams there are some particular values $\mathcal{L}_{lm}$ determined by all the maxima of the intensity pattern of the Bessel beam of order m. In exactly the same way all the maxima of the intensity pattern of the vectorial Bessel beam of order m will determine some values $\mathcal{L}^p_{lm}$. We believe that the parameter $\mathcal{P} \equiv \mathcal{L}^p_{lm} - \mathcal{L}_{lm}$ gives a characterization of the polarization of the vectorial optical field. We will study in detail this suggestion in a future work.

Along the work in chapter 3, we have computed the reflection of a plane wavefront by a parabolical mirror and the corresponding ronchigram. That is, we have obtained expressions for: the incident light rays and wavefronts, the reflected light rays, the reflected wavefronts, the caustic and the ronchigram. Those general results were applied to the antenna of the LMT/GTM to study the behavior of the reflected light rays, reflected wavefronts, caustic and ronchigram for an incident plane wave evolving along the $-\sin\pi/10\,\hat{x} - \cos\pi/10\,\hat{z}$ direction. We have shown that the caustic has a singularity of the hyperbolic umbilic type, which is locally stable under small perturbations of the optical system. Furthermore, we have presented plots of the distribution of the reflected light rays on the planes $z = 15\,m$, $z = 17.5\,m$ and $z = 20\,m$, when the incident plane wave is evolving along the directions $-\sin\pi/200\,\hat{x} - \cos\pi/200\,\hat{z}$ and $-\sin\pi/10\,\hat{x} - \cos\pi/10\,\hat{z}$. From the results obtained in Fig. (3.4) and Fig. (3.5) we conclude that among all the radiation reflected by the antenna of the LMT/GTM, the portion of that radiation which enters to the detector to be analyzed is that which has an angle $\alpha \approx 0$. The results presented in this work, could be associated to the radiation of a static source, in the geometrical optics limit. For a distant source emitting radiation in the observable universe, a plane wavefront would arrive with a certain inclination to the detector of the antenna. From the information collected at the focal region, a ronchigram can be generated and to indicate whether the emitting source is static or not. Ronchigrams such as those shown in Figs. (3.7) and (3.8), are patterns that indicate the presence of a static source.

The results presented here in chapter 3 are the basis to compute the reflection of a Bessel beam of order m by the antenna of the LTM/GTM by using the scalar wave equation and the geometrical optics point of view. That is, we are interested in computing the reflected light rays, reflected wavefronts, caustic and the intensity pattern associated with the reflection of a Bessel beam of the order m by the antenna of the LMT/GTM. That computation is important because the intensity pattern associated with the reflection of a vortex Bessel beam of order m could be associated with the reflection of the radiation emitted by a rotating celestial high energy source, which is our major aim in the near future.

Here anew, we remark that: the idea of relate the intensity pattern associated with the reflection of a Bessel beam of order m, asymptotically, to the radiation emitted by a point-like source in the vicinity of a Kerr black hole, is a very strong **hypothesis**, and that the basis of this strong assumption is that modeling the radiation to be detected as a beam of vortex kind, is an acceptable approximation for the first steps of this project. Thus, we take the simplest case of that class of beam, which is the Bessel beam of order m.

Along of this line of research there has been important contributions on the reflection and refraction of the so called non diffracting beams in the paraxial approximation [30, 43, 44]. Furthermore there has been research studies about reflection on parabolic mirrors, for example, describing the electromagnetic or electric field respectively, to show that in the vicinity of the focus, a segment of the paraboloid produces an intensity distribution that is identical to that obtained from a far-field-type approximation, for a lossless rotational paraboloid mirror [45] and to show that, when the mirror is illuminated with a beam having a nonzero angle of incidence, whose axis of propagation does not exactly coincide with the axis of revolution of the mirror, there is a distortion and strong coma [46].

Finally in chapter 4, by using the Kirchhoff's integral applied to a parabolical mirror an integral expression for the scalar optical field associated with the reflection of a Bessel beam of order m was obtained. Furthermore, under certain approximation we have derived an analytical expression for the intensity pattern associated with the reflection of a Bessel beam of order m by the LMT/GTM antenna. This general result has been applied to the special cases of a Bessel beam of zero order and $m = 5$ for some particular values of $\tilde{Z} = 50, 100$ and $\alpha = \pi/100, \pi/10$. From the preliminar results shown in chapter 4, could be possible to make the difference between the radiation emmited by a puntual source in the vicinity of the enven horizon of a Schwarzschild black hole ($m = 0$) and that of the Kerr black hole ($m \neq 0$). It is important to emphazise that more accurated results for the intensity pattern associated with the reflection of a Bessel beam of order m by the LMT/GTM antenna is obtained by using the scalar optical field given by Eq. (4.30), which is valid for any value of (τ, θ, Z). Furthermore, it is important to remark that in Eq. (4.39) we are only considering the intensity associated with the reflection of a Bessel beam of order m without taking into account the interference between the reflected field by the parabolical antenna and the incident Bessel beam of order m. The implementation of these improvements in the study of the reflection of a Bessel beam of order m by the LMT/GTM antenna, are part of the research in near future.

Bibliography

[1] O. de J. Cabrera-Rosas, E. Espíndola-Ramos, S. A. Juárez-Reyes, I. Julián-Macías, P. Ortega-Vidals, G. Silva-Ortigoza, R. Silva-Ortigoza, and C. T. Sosa-Sánchez, *Wavefronts and caustic associated with Durnin's beams*, J. Opt. **19** (2017) 015603.

[2] C. T. Sosa-Sánchez, G. Silva-Ortigoza, S. A. Juárez-Reyes, O. de J. Cabrera-Rosas, E. Espíndola-Ramos, I. Julián-Macías, and P. Ortega-Vidals, *Parabolic non-diffracting beams: geometrical approach*, J. Opt. **19** (2017) 085604.

[3] I. Julián-Macías, C. Rickenstorff-Parrao, O. de J. Cabrera-Rosas, E. Espíndola-Ramos, S. A. Juárez-Reyes, P. Ortega-Vidals, G. Silva-Ortigoza, and C. T. Sosa-Sánchez, *Wavefronts and caustics associated with Mathieu beams*, J. Opt. Soc. Am. A, **35** (2018) 267-274.

[4] A. González-Juárez and G. Silva-Ortigoza, *Curves, wavefronts and caustics determined by the intensity pattern of an adiffractional beam*, Phys. Scr. **94**, (2019) 055505.

[5] P. Treviño, O. López-Cruz, and Chávez-Cerda, *Segmented vortex telescope and its tolerance to diffraction effects and primary aberrations*, Optical Engineering. **52**, (2013) 081605.

[6] F. Tamburini, B. Thidé, G. Molina-Terriza, and G. Anzolin, *Twisting of light around rotating black holes*, Nature. Phys. **7**, (2011) 195-197.

[7] A. González-Juárez, G. Silva-Ortigoza, and E. Espíndola-Ramos, *Geometric treatment of the radiation captured by the Large Millimeter Telescope (LMT/GTM) and ronchigrams at the caustic region for a static source*, J. Opt. **23** (2021) 015603.

[8] J. Durnin, *Exact solutions for nondiffracting beams. I. The scalar theory*, J. Opt. Soc. Am. A, **4** (1987) 651-654.

[9] J. E. Durnin, J. J. Miceli, and J. H. Eberly, *Diffraction-Free Beams*, Phys. Rev. Lett. **58** (1987) 1499-1501.

[10] D. McGloin and K. Dholakia, *Bessel beams: diffraction in a new light*, Contemp. Phys. **46** (2005) 15-28.

[11] H. Rubinsztein-Dunlop, A. Forbes, M. V. Berry, M. R. Dennis, D. L. Andrews, M. Mansuripur, C. Denz, C. Alpmann, P. Banzer, T. Bauer, E. Karimi, L. Marrucci, M. Padgett, M. Ritsch-Marte, N. M. Litchinitser, N. P. Bigelow, C. Rosales-Guzmán, A. Belmonte, J. P. Torres, T. W. Neely, M. Baker, R. Gordon, A. B. Stilgoe, J. Romero, A. G. White, R. Fickler, A. E. Willner, G. Xie, B. McMorran, and A. M Weiner, *Roadmap on structured light*, J. Opt. **19** (2017) 013001.

[12] J. C. Gutiérrez-Vega, M. D. Iturbe-Castillo, and S. Chávez-Cerda, *Alternative formulation for invariant optical fields: Mathieu beams* Opt. Lett. **25** (2000) 1493-1495.

[13] S. Chávez-Cerda, J. C. Gutiérrez-Vega, and G. H. C. New, *Elliptic vortices of electromagnetic wave fields* Opt. Lett. **26** (2001) 1803-1805.

[14] J. C. Gutiérrez-Vega, M. D. Iturbe-Castillo, G. A. Ramírez, E. Tepichín, M. R. Rodríguez-Dagnino, S. Chávez-Cerda, and G. H. C. New, *Experimental demonstration of optical Mathieu beams*, Opt. Commun. **195** (2001) 35-40.

[15] M. A. Bandres and J. C. Gutiérrez-Vega, *Parabolic nondiffracting optical wave fields*, Opt. Lett. **29** (2004) 44-46.

[16] C. P. Boyer, E. G. Kalnins, and W. Miller, *Symmetry and separation of variables for the Helmholtz and Laplace equations*, Nagoya Math. J. **60** (1976) 35-80.

[17] S. Vo, K. Fuerschbach, K. P. Thompson, M. A. Alonso, and J. P. Rolland, *Airy beams: a geometric optics perspective*, J. Opt. Soc. Am. A, **27** (2010) 2574-2582.

[18] R. Grunwald and M. Bock *Propagation and wavefront ambiguity of linear nondiffracting beams*, Proceedings Volume 8999, Complex Light and Optical Forces VIII; 89990G (2014) (https://doi.org/10.1117/12.2037045).

[19] D. G. Burkhard and D. L. Shealy, *Flux density for ray propagation in geometrical optics*, J. Opt. Soc. Am. **63** (1973) 299-304.

[20] P. Ortega-Vidals, O. de J. Cabrera-Rosas, E. Espíndola-Ramos, S. A. Juárez-Reyes, I. Julián-Macías, G. Silva-Ortigoza, R. Silva-Ortigoza, and C. T. Sosa-Sánchez, *Wavefronts, caustic, and intensity of a plane wave refracted by an arbitrary surface: the axicon and the plano spherical lenses*, J. Opt. Soc. Am. A, **34** (2017) 1679-1678.

[21] V. I. Arnold, S. M. Gusein-Zade and A. N. Varchenko, *Singularities of Differentiable Maps* Vol I, (Birkhäuser, Boston, 1995).

[22] V. I. Arnold, *Singularities, bifurcations, and catastrophes*, Usp. Fiz. Nauk **141** (1983) 569-590.

[23] O. de J. Cabrera-Rosas, E. Espíndola-Ramos, S. A. Juárez-Reyes, I. Julián-Macías, P. Ortega-Vidals, C. Rickenstorff-Parrao, G. Silva-Ortigoza, R. Silva-Ortigoza, and C. T. Sosa-Sánchez, *Durnin-Whitney beams*, J. Opt. **19** (2017) 055606.

[24] Yu. A. Kravtsov and Yu. I. Orlov, *Geometrical Optics of Inhomogeneous Media*, Springer-Verlag, 1990.

[25] M. V. Berry, *Waves and Thom's theorem*, Advances in Physics **25** (1976) 1-26.

[26] M. V. Berry and C. Upstill, *Catastrophe optics: morphologies of caustics and their diffraction patterns*, Progress in Optics **XVIII** (1980) 257-346.

[27] N. Yu, P. Genevet, M. A. Kats, F. Aieta, F. Capasso, and Z. Gaburro, *Light Propagation with Phase Discontinuities: Generalized Laws of Reflection and Refraction*, SCIENCE **334** (2011) 333-337.

[28] S. A. Juárez-Reyes, C. T. Sosa-Sánchez, G. Silva-Ortigoza, O. de J. Cabrera-Rosas, E. Espíndola-Ramos, and P. Ortega-Vidals, *The wire optical test: a thorough analytical study in and out of caustic surface, and advantages of a dynamical adaptation*, J. Opt. **20** (2018) 035602.

[29] S. A. Juárez-Reyes, C. T. Sosa-Sánchez, G. Silva-Ortigoza, O. de J. Cabrera-Rosas, E. Espíndola-Ramos, and I. Julián-Macías, *Approaching all the configurations for the analytical ronchigram in relation to the caustic region for an arbitrary plank-convex lens*, J. Opt. **20** (2018) 075611.

[30] I. Julián Macías, C. T. Sosa-Sánchez, O. de J. Cabrera-Rosas, E. Espíndola-Ramos, and G. Silva-Ortigoza, *The vector Durnin-Whitney beam*, J. Opt. Soc. Am. A, **37** (2020) 294-304.

[31] J. J. Wang, T. Wriedt, J. A. Lock, and L. Madler, *General description of circularly symmetric Bessel beams of arbitrary order*, Journal of Quantitative Spectroscopy and Radiative, **184** (2016) 218-232.

[32] F. G. Mitri, R. X. Li, R. P. Yang, L. X. Guo, and C. Y. Ding, *Optical pulling force on a magneto-dielectric Rayleigh sphere in Bessel tractor polarized beams*, Journal of Quantitative Spectroscopy and Radiative, **184** (2016) 360-381.

[33] F. G. Mitri, *Reverse propagation and negative angular momentum density flux of an optical nondiffracting nonparaxial fractional Bessel vortex beam of progressive waves*, J. Opt. Soc. Am. A, **33** (2016) 1661-1667.

[34] EHT Collaboration, *First M87 Event Horizon Telescope Results. I. The Shadow of the Supermassive Black Hole*, ApJL **875**, (2019) L1.

[35] EHT Collaboration,*First M87 Event Horizon Telescope Results. II. Array and Instrumentation*, ApJL **875**, (2019) L2.

[36] N. Bretón, O. de Jesús Cabrera-Rosas, E. Espíndola-Ramos, S. A. Juárez-Reyes, I. Julián-Macías, A. Montiel, P. Ortega-Vidals, E. Román-Hernández, G. Silva-Ortigoza, R. Silva-Ortigoza, C. T. Sosa-Sánchez, and R. Suárez-Xique, *Towards the Ronchi test for gravitational lenses: the gravitoronchigram*, J. Opt. **19**, (2017) 065602.

[37] V. I. Arnold, *Mathematical Methods of Classical Mechanics*, Springer-Verlag, 1974.

[38] E. Román-Hernández, J. G. Santiago-Santiago, G. Silva-Ortigoza, and J. Velázquez Castro, *Describing the structure of ronchigrams when the grating is placed at the caustic region: The paraboloical mirror*, J. Opt. Soc. Am A **27**, (2010) 832-845.

[39] A. Cordero-Davila, A. Cornejo-Rodriguez, and O. Cardona-Nuñez, *Ronchi and Hartmann tests with the same mathematical theory*, Applied Optics **31**, (1992) 2370-2376.

[40] S. M. G. Z. V. I. Arnold and A. N. Varchenko, *Singularities of Differentiable Maps*, Birkhäuser, 1995.

[41] V. I. Arnold, *Singularities, bifurcations, and catastrophes*, Usp. Fiz. Nauk **141**, (1983) 569-90.

[42] J. Castro-Ramos, S. A. Juárez-Reyes, M. Marcelino-Aranda, P. Ortega-Vidals, G. Silva-Ortigoza, R. Silva-Ortigoza, and R. Suárez-Xique, *The refraction and reflection laws from a complete integral of the eikonal equation and Huygens' principle*, J. Opt. **17**, (2015) 015601.

[43] M. A. Bandres and M. Guizar-Sicairos, "Paraxial group", Opt. Lett. **34**, (2008) 13-15.

[44] R. I. Hernandez-Aranda, J. C. Gutiérrez-Vega, M. Guizar-Sicairos, and M. A. Bandres, *Propagation of generalized vector Helmholtz-Gauss beams through paraxial optical systems*, Opt. Express **14**, (2006) 8974-8988.

[45] P. Varga and P. Török, *Focusing of electromagnetic waves by paraboloid mirrors. II. Numerical results*, J. Opt. Soc. Am A **17**, (2000) 2090-2095.

[46] P. Bilodeau and M. Piché, *Focusing a TM_{01} beam with a slightly tilted parabolic mirror*, Opt. Express **19**, (2011) 9201-9212.

[47] W. Emil and B. Max, *Principles of Optics*, Pergamon, 1959.